British Journal of Pharmacology

DOI:10.1111/j.1476-5381.2011.01771.x
www.brjpharmacol.org

RESEARCH PAPER

Reversed binding of a small molecule ligand in homologous chemokine receptors – differential role of extracellular loop 2

PC Jensen[1], S Thiele[1], A Steen[1], A Elder[2]*, R Kolbeck[2]*, S Ghosh[2]*, TM Frimurer[3] and MM Rosenkilde[1]

[1]*Department of Neuroscience and Pharmacology, Copenhagen University, Copenhagen, Denmark,* [2]*Millennium Pharmaceuticals, Cambridge, MA, USA, and* [3]*Center for Protein Research, Faculty of Health Sciences, Copenhagen University, Copenhagen, Denmark*

Correspondence
Mette M Rosenkilde, Department of Neuroscience and Pharmacology, Copenhagen University, Blegdamsvej 3, Buildn 18.6, Copenhagen DK-2200, Denmark. E-mail: rosenkilde@sund.ku.dk

*Present address: Galenea Corp., Cambridge, Massachusetts (AE), Pharmaceuticals Inc., Cambridge, Massachusetts (SG) and MedImmune, Gaithersburg, Maryland (RK).

Keywords
chemokine receptors; small molecule agonist; reversed binding; extracellular loop 2

Received
3 February 2011
Revised
19 September 2011
Accepted
26 September 2011

BACKGROUND AND PURPOSE

The majority of small molecule compounds targeting chemokine receptors share a similar pharmacophore with a centrally located aliphatic positive charge and flanking aromatic moieties. Here we describe a novel piperidine-based compound with structural similarity to previously described CCR8-specific agonists, but containing a unique phenyl-tetrazol moiety which, in addition to activity at CCR8 was also active at CCR1.

EXPERIMENTAL APPROACH

Single point mutations were introduced in CCR1 and CCR8, and their effect on small molecule ligand-induced receptor activation was examined through inositol trisphosphate (IP_3) accumulation. The molecular interaction profile of the agonist was verified by molecular modeling.

KEY RESULTS

The chemokine receptor conserved glutamic acid in TM-VII served as a common anchor for the positively charged amine in the piperidine ring. However, whereas the phenyl-tetrazol group interacted with TyrIV:24 (Tyr^{172}) and TyrIII:09 (Tyr^{114}) in the major binding pocket (delimited by TM-III to VII) of CCR8, it also interacted with TrpII:20 (Trp^{90}) and LysII:24 (Lys^{94}) in the minor counterpart (delimited TM-I to III, plus TM-VII) in CCR1. A straightening of TM-II by Ala-substitution of ProII:18 confirmed its unique role in CCR1. The extracellular loop 2 (ECL-2) contributed directly to the small molecule binding site in CCR1, whereas it contributed to efficacy, but not potency in CCR8.

CONCLUSION AND IMPLICATIONS

Despite high ligand potency and efficacy and receptor similarity, this dual-active and bitopic compound binds oppositely in CCR1 and CCR8 with different roles of ECL-2, thereby expanding and diversifying the influence of extracellular receptor regions in drug action.

Abbreviations

4D, four-dimensional; 7TM receptors, 7 transmembrane receptors; CCD, cyclic coordinate descent; EBI2, Epstein–Barr virus-induced receptor 2; ECL, extracellular loop; IP, inositol phosphate; KIC, kinematic loop closure; LMD-559-1-(3-(2-chlorophenoxy)benzyl)-4-(5-chloro-2-(1*H*-tetrazol-5-yl)phenyl)piperidin-4-ol; TM, transmembrane; WT, wild type

Introduction

Chemokines constitute a class of small chemoattractant cytokines comprising approximately 50 members. Structural hallmarks divide these members into four groups dependent on the spacing between the first two (of usually four) conserved cysteines: (1) CCL1-28; (2) CXCL1-16; (3) XCL1; and (4) CX_3CL1. The chemokine receptors belong to the rhodopsin-like 7 transmembrane (7TM) GPCRs and are divided into four corresponding groups, depending on their preferred endogenous ligand(s). A notable trait of the chemokine system is a high level of promiscuity that allows a single chemokine to target several receptors and for a single receptor to bind several different chemokines (Murphy *et al.*, 2000).

The chemokine receptor CCR8, however, is monogamous in its interaction with CCL1 (I-309),i.e. CCL1 is the only endogenous ligand for CCR8, and CCL1 only binds to this receptor (receptor nomenclature follows Alexander *et al.*, 2011). It is mainly expressed in CD4-positive T cells, preferentially in T_H2 cells (Zingoni *et al.*, 1998), and is therefore involved in conditions such as asthma, atopic dermatitis and anaphylaxis (Gombert *et al.*, 2005). Consequently, much effort has been expended in the discovery of clinically useful CCR8 antagonists but without much success, as high-throughput screenings have primarily identified agonists (Haskell *et al.*, 2006). Thus, we have previously described the identification and interaction of four CCR8-selective small molecule agonists (LMD-009, -584, -268 and -174; Figure 1B), acting with potencies and efficacies similar to CCL1 (Jensen *et al.*, 2007). Despite the agonist-prone nature of CCR8, small molecule antagonists have been described (Jenkins *et al.*, 2007). The structurally closest human homologue of CCR8 is CCR1, which is targeted by at least two endogenous chemokines (CCL3 and CCL5) and for which several non-peptide agonists and antagonists have been described (Hesselgesser *et al.*, 1998; Liang *et al.*, 2000; de Mendonca *et al.*, 2005; Vaidehi *et al.*, 2006; Jensen *et al.*, 2008).

A common pharmacophore for most non-peptide antagonists targeting CC-chemokine receptors describes a centrally

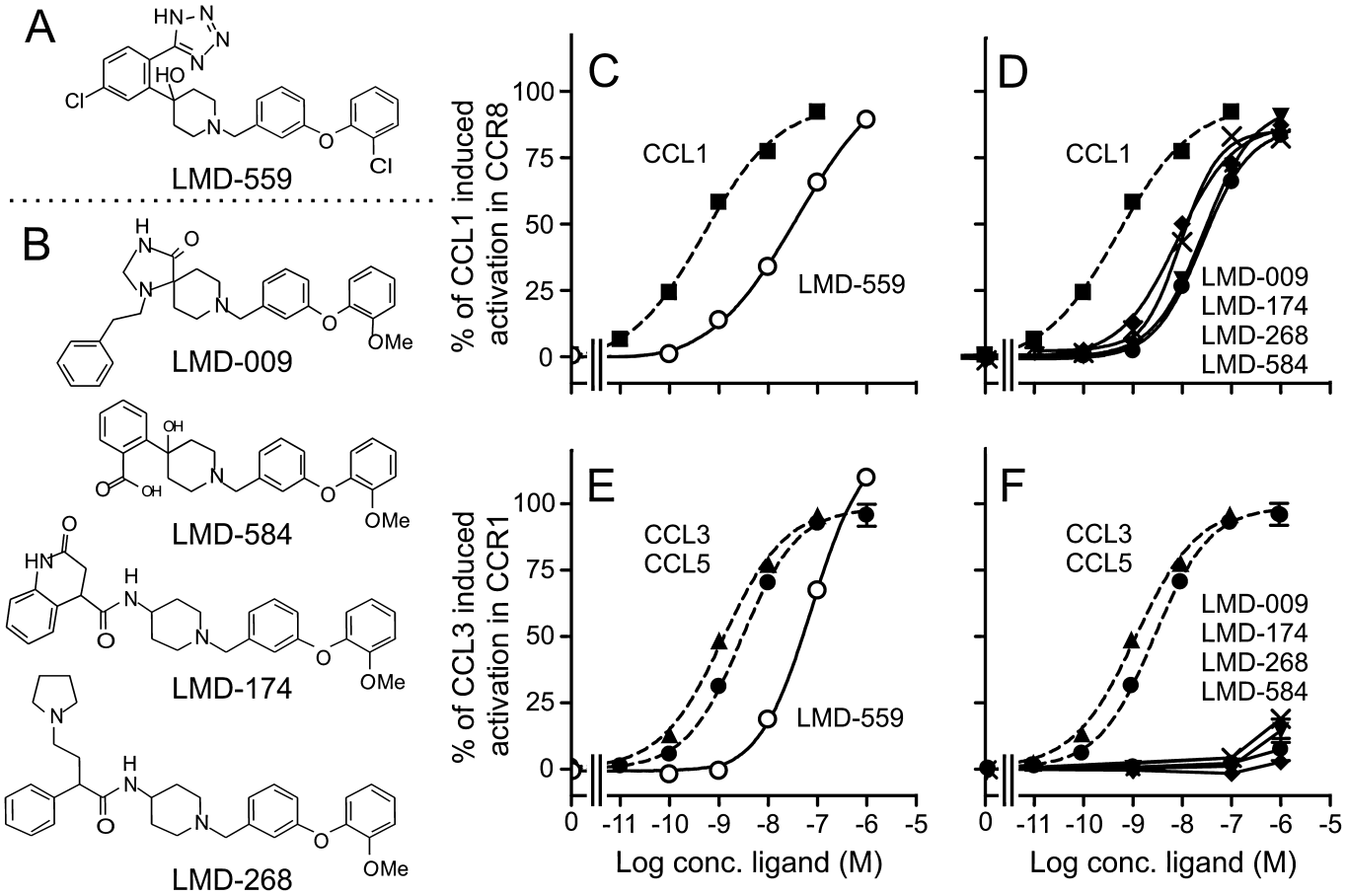

Figure 1

Dual activation of CCR1 and CCR8 by LMD-559. The tetrazol-containing piperidine-based compound LMD-559 activates CCR1 and CCR8 with nanomolar potencies. (A) Structure of LMD-559. (B) Structures of the previously described CCR8-selective agonists: LMD-009, LMD-584, LMD-174 and LMD-268 (Jensen *et al.*, 2007). (C–F) IP_3 accumulation experiments performed in transiently transfected COS-7 cells. The endogenous ligands CCL1, CCL3 and CCL5 are shown on CCR8 (C,D) and CCR1 (E,F) respectively. Activation by LMD-559 in CCR8 (C) and CCR1 (E) are shown together with the activation by LMD-584, LMD-174, LMD-268 and LMD-009 in CCR8 (D – as previously published) (Jensen *et al.*, 2007) and in CCR1 (F) (n = 10–63).

located, positively charged, nitrogen and flanking aromatic moieties. These ligands match a common tertiary structure in most chemokine receptors, with a conserved negatively charged Glu in the top of TM-VII (position VII:06/7.39; note that we use the residue numbering system described by Baldwin (Baldwin, 1993; Schwartz, 1994) and, for the first time a certain residue is mentioned, we also show the numbering according to Ballesteros and Weinstein (1995). This negatively charged residue provides a bridge between, and divides, the main ligand-binding pocket into a major and minor component, characterized by aromatic environments in both pockets (Rosenkilde and Schwartz, 2006; Jensen and Rosenkilde, 2009; Rosenkilde *et al.*, 2010). This division was indeed indicated by the very recently published first crystal structure of a chemokine receptor (CXCR4), which may represent the structure of chemokine receptors in general. In this structure, especially the helices confining the minor binding pocket (TM-I, II and III) are changed in rotation and localization relative to the previously published crystal structures of other rhodopsin-like 7TM receptors (adenosine A_{2A} receptors, β_1- and β_2 adrenoceptors and rhodopsin itself) (Palczewski *et al.*, 2000; Cherezov *et al.*, 2007; Jaakola *et al.*, 2008; Scheerer *et al.*, 2008; Warne *et al.*, 2008; Wu *et al.*, 2010).

Despite major chemical differences between endogenous ligands (ions, monoamines, lipids, peptides and glycoproteins) and between non-peptide ligands targeting 7TM receptors, it is believed that receptor activation occurs through common mechanisms involving a series of microswitches that overall result in outward movements of especially TM-VI on the intracellular side and inward movements of this helix on the extracellular side (Elling and Schwartz, 1996; Farrens *et al.*, 1996; Hubbell *et al.*, 2003; Nygaard *et al.*, 2009). The overall properties of this model have been verified by crystal structures of both active and inactive receptors (Palczewski *et al.*, 2000; Cherezov *et al.*, 2007; Jaakola *et al.*, 2008; Scheerer *et al.*, 2008; Warne *et al.*, 2008; Wu *et al.*, 2010) and by the latest published crystal structures of agonist-bound β_1- and β_2-adrenoceptors (Rasmussen *et al.*, 2011; Warne *et al.*, 2011). These structures also revealed how the extracellular loop 2 (ECL-2) – in particular region ECL-2B (the C-terminal part of ECL-2 from the conserved Cys to the start of TM-V) – forms a lid over the main binding pocket and in fact may participate directly in the binding of small ligands anchoring in the main ligand-binding pocket (Peeters *et al.*, 2011).

Here we describe a novel non-peptide CCR agonist, LMD-559, consisting of a phenoxybenzyl piperidine core structure (Figure 1A) and very similar to the previously characterized CCR8-selective agonists (Figure 1B) (Jensen *et al.*, 2007). However, a unique feature of LMD-559 is the phenyl-tetrazol group ('left' side of the molecule) that changes the CCR8 selectivity towards a dual activation of CCR8 and CCR1. By employing a series of mutations confining the main ligand-binding pockets of CCR1 and CCR8 and in extracellular regions, combined with molecular modelling, we showed that the dually active compound interacted differently – in fact, oppositely, in a mirrored manner centred around Glu-VII:06 – with these two receptors. Analysis of the role of the ECL-2 showed that the ECL-2B region contributed to the potency of LMD-559 in CCR1 as a part of the binding site whereas, in CCR8, this region contributed to the efficacy (but not the potency) of small molecule as well as chemokine agonists, indicating an indirect role in constraining the receptor in an active conformation(s).

Methods

Site-directed mutagenesis

Point mutations were introduced using the PCR overlap extension technique with human CCR1 WT and CCR8 WT as templates. All reactions were carried out using the Pfu polymerase (Stratagene, Santa Clara, CA, USA). The mutant receptors were cloned into the eukaryotic expression vector pcDNA3.1 and were all verified by DNA sequencing.

Transfections and tissue culture

COS-7 cells were grown at 10% CO_2 and 37°C in Dulbecco's modified Eagle's medium with glutamax (Gibco, cat. no. 21885-025, Grand Island, NY, USA) adjusted with 10% fetal bovine serum, 180 $\mu g \cdot mL^{-1}$ penicillin and 45 $\mu g \cdot mL^{-1}$ streptomycin (PenStrep). CHO cells stably expressing CCR1 were grown at 5% CO_2, 37°C in RPMI-1640 medium with glutamine supplemented with 10% fetal bovine serum, 180 $\mu g \cdot mL^{-1}$ penicillin and 45 $\mu g \cdot mL^{-1}$ streptomycin. Transfection of COS-7 cells was performed by the calcium phosphate precipitation method (Rosenkilde *et al.*, 1994).

Inositol trisphosphate assay (IP_3 turnover)

COS-7 cells were transfected as described above. The co-transfection with the chimeric G protein Gqi4myr turns the $G\alpha_i$ signal into a $G\alpha_q$ signal, making it possible to measure the chemokine receptor activation as IP turnover (Heydorn *et al.*, 2004). One day after transfection, the cells were seeded in 24-well plates (1.5×10^5 cells per well) and incubated with 2 µCi of ^{3}H-*myo*-inositol in 0.3 mL growth medium for 24 h. Cells were washed twice with HBSS supplemented with $CaCl_2$ and $MgCl_2$ (Gibco14025) and afterwards incubated for 15 min in 0.3 mL buffer supplemented with 10 mM LiCl prior to ligand addition followed by 90 min incubation. When used, the antagonists were added 10 min prior to the agonist. The generated $[^3H]IP_3$ was purified on AG 1X8 anion exchange resin. Determinations were made in duplicate.

Chemotaxis

Chemotaxis was carried out on THP-1 cells kindly provided by Dr HR Lüttichau. The cells were washed once and suspended in chemotaxis buffer (RPMI-1640 supplemented with 0.5% BSA) and loaded in the filters of Transwell chemotaxis plates (3.0 µm polycarbonate membrane, Costar, Lowell, MA, USA) at 10^6 cells per 100 µL per filter. Antagonists were added to the cells in the upper chamber followed by 15 min incubation. The agonists were added to the lower chamber (10 nM of CCL1 and CCL5 and 100 nM of LMD-559), followed by 3.5 h incubation at 5% CO_2, 37°C. The migrated cells were counted by FACS.

Intracellular calcium levels

CHO cells stably expressing CCR1 were incubated in RPMI-1640 1% FBS supplemented with FURA-2AM (Molecular Probes, Eugene, OR) for 30 min. at 37°C. Aliquots were made of 1×10^6 cells and re-suspended in 500 µL PBS containing 1%

FBS and 10 mM EGTA. Fluorescence was measured on a Jobin Yvon Flouromax-2 (Jobin Yvon Spex, Cedex, France).

ELISA for surface receptors

COS-7 cells were transiently transfected with N-terminal M1 FLAG-tagged CCR1 and CCR8 receptors, and seeded in 96-well plates (35 000 cells per well). The cells were washed once in TBS (50 mM Tris-base, 150 mM NaCl, pH 7.6) and subsequently fixed in 150 μL 4% formaldehyde for 15 min. After three washes in TBS, the cells were blocked in TBS containing 2% BSA for 30 min. Subsequently, the cells were incubated with mouse M1 anti-FLAG antibody 2 $\mu g \cdot mL^{-1}$ in TBS containing 1% BSA and 1 mM $CaCl_2$ for 2 h. Following three washes in TBS with 1 mM CaCl, the cells were incubated with goat anti-mouse horseradish peroxidase-conjugated IgG antibody diluted 1:1000 in TBS containing 2% BSA and 1 mM $CaCl_2$ for 1 h. After three washes in TBS, the immunoreactivity was revealed by addition of horseradish peroxidase substrate, according to the manufacturer's instructions.

Molecular modelling

The protein modelling package in sybylx1.2 was used to construct initial comparative homology models of the target receptors CCR1 and CCR8. Initially, the FUGUE™ technology (Shi *et al.*, 2001; Williams *et al.*, 2001) was used to identify structural homologs of the target sequences through sequence–structure comparison using a database of structural profiles (derived from the structural alignments of experimentally determined protein structures in homologous structure alignment database (HOMSTRAD™), a database containing 3D protein structures clustered into families) (Mizuguchi *et al.*, 1998) of known protein families represented by environment-specific substitution table that takes into account secondary structure, solvent accessibility and hydrogen-bonding interactions, and structure-dependent gap penalties. As expected, CXCR4 followed by β_2-adrenoceptor was identified as preferred templates for CCR1 and CCR8 modelling. Homology models of CCR1 and CCR8 were constructed from pair-wise sequence alignment between CCR1, CCR8, the X-ray template structures of β_2-adrenoceptors (PDB entry 2RH1) (Cherezov *et al.*, 2007) and the CXCR4 receptor (Wu *et al.*, 2010) using the biopolymer modules (ORCHESTRAR) in sybylx1.2, which can use structural information from multiple homolog templates. The resulting CCR1 and CCR8 receptor models were subsequently relaxed 500 times in Rosetta 3.1 simulations (Barth *et al.*, 2009) using the relax protocol and Rosettas full atom force field to repack side chains and refine the extracellular loops to obtain energetically favourable structures for docking. The extracellular loops (ECL-1, -2 and -3) was optimized 1000 times in a subsequent loop refinement protocol starting from the lowest energy structures using the cyclic coordinate descent (CCD) (Canutescu and Dunbrack, 2003; Wang *et al.*, 2007) followed by kinematic loop closure (KIC) (Coutsias *et al.*, 2005; Mandell *et al.*, 2009) loop modelling that uses a simulated annealing Metropolis Monte Carlo protocol to refine (local perturbations refine kic mode) for the extracellular loops. During the model refinements, a disulphide bridge between Cys^{106} (position III:01) and Cys^{183} in the ECL-2B loop (same number in both receptors) was applied as a structural constraint. Otherwise, loops were modelled *ab initio*. The best CCR1 and CCR8 models were finally relaxed 500 times. A set of representative CCR1 and CCR8 models was selected based on energy and structural diversity. Finally, we performed four-dimensional (4D) docking simulation that allows seamless incorporation of an ensemble of receptor models to represent the conformational variability of the binding pockets and indirectly take account of the binding pocket flexibility and induced fit. Specifically, a fully flexible docking of LMD-559 to an example of CCR1 and CCR8 receptor models, was performed by ICM BPMC under softened van der Waals conditions using 4D grids represented by six grid potentials of 0.5 Å spacing, including three van der Waals grid potentials for a carbon probe, large atom probe or hydrogen probe, a hydrogen bonding grid potential, an electrostatic grid potential and a hydrophobic grid potential ICM (Totrov and Abagyan, 2008; Bottegoni *et al.*, 2009). The docking grids were defined to encompass a binding pocket described by all corresponding receptor residues within 4.5 Å of the ligands in the template crystal structures. Individual best scored docking poses were subsequently optimized using a combined Monte Carlo and minimization procedure (using the MMFF94 force field), keeping ligand and surrounding protein residues (in an 8 Å radius from the starting position) flexible. All backbone coordinates were held fixed. Two rounds of optimization were performed: an initial refinement under a softened van der Waals (vdW potential and a second refinement with the full van der Waals potential. A final stack of 50 conformations was generated, which were scored and analysed to identify the best fit.

Statistical analysis

Statistical analysis was performed in Excel. Analysis of significance in fold change of potencies of LMD-559 activation of mutant receptors was carried out using the two-sample *t*-test. A *P*-value of less than 0.05 (95% confidence interval) was considered as statistically significant.

Materials

The human chemokines CCL1, CCL3 and CCL5 were purchased from Peprotech (Rocky Hill, NJ, USA). Human chemokine receptor cDNA was kindly provided by Tim Wells (Serono Pharmaceutical Research Institute, Geneva, Switzerland) or purchased from Origene (Rockville, MD). ^{3}H-*myo*-Inositol (PT6-271) and iodinated chemokines (^{125}I-CCL3 and ^{125}I-CCL5) were purchased from Amersham Pharmacia Biotech (Uppsala, Sweden). The promiscuous chimeric G-protein GαΔ6qi4myr (abbreviated Gqi4myr), was kindly provided by Evi Kostenis (University of Bonn, Germany). AG 1-X8 anion-exchange resin was purchased from Bio-Rad Laboratories (Hercules, CA, USA).

Results

As expected from the similar pharmacophores of LMD-559 (Figure 1A) and of previously characterized CCR8-selective compounds (Figure 1B) (Jensen *et al.*, 2007), the tetrazol-containing ligand (LMD-559) acted as a full agonist on CCR8 (Figure 1C) with high potency, equal to that of the other

CCR8-selective compounds (Figure 1D). All endogenous chemokine receptors were subsequently tested and surprisingly, LMD-559 activated CCR1 in addition to CCR8 (Figure 1E, Table 1), but not any other receptor – except for a minor activation at 1 μM for CCR3 (Figure S1). The compound was subsequently tested for antagonistic properties on all endogenous chemokine receptors but no such effect was observed (Figure S2). As the IP_3 accumulation experiments are based on co-transfection with a promiscuous chimeric Gα-subunit (Gqi4myr) that is recognized as a $G\alpha_i$ subunit, but transduces a $G\alpha_q$ signal (Heydorn *et al.*, 2004), LMD-559 was tested for its ability to induce more natural signalling pathways via CCR1. Supporting the IP_3 accumulation experiments, LMD-559 induced calcium release in stably transfected CHO cells (Figure 2A) with an efficacy similar to CCL3 (Figure 2B). Furthermore, it induced chemotaxis of the human monocytic cell line THP-1 with a classical bell-shaped dose–response curve, again being as efficacious as CCL3 (Figure 2C). Importantly, the migration induced by LMD-559 was completely repressed by the CCR1 antagonist vMIP-II. Note that although vMIP-II is a broad-spectrum chemokine receptor antagonist, it crucially does not block CCR8 (Kledal *et al.*, 1997; Luttichau *et al.*, 2000). The migration was also unchanged by the CCR8-specific antagonist MC-148, confirming that the migration induced by LMD-559 in THP-1 cells was due to CCR1 activation (Figure 2D). The level of CCR8 expression in monocytes is known to be very low (Patel *et al.*, 2001; Phillips *et al.*, 2005). As the physiological response is not necessarily proportional to occupancy, it is possible that CCL1 displays the same efficacy through CCR8 as CCL3 elicits through CCR1 despite the presence of only few CCR8 receptors.

To rule out the possibility that the previously described CCR8-specific agonists (LMD-009, -584 -174 and -268 in Figure 1B) still bound to CCR1 without acting as agonists, we tested whether they could inhibit the action of LMD-559. However, despite similar core structures, LMD-009, -584 -174 and -268 were not antagonists of LMD-559 at CCR1, indicating that these compounds in fact did not bind to CCR1 (data not shown). Thus, in spite of a very similar pharmacophore of all CCR8-activating compounds (Figure 1), the tetrazol moiety conferred dual activity towards CCR1 and CCR8. To further characterize the binding mode of LMD-559, we carried out competition binding experiments against ^{125}I-CCL3 and ^{125}I-CCL5 at CCR1, and ^{125}I-CCL1 at CCR8. We found that LMD-559 was not able to compete with CCL1 at CCR8 (Figure 3C), and that the affinity for competition at CCR1 was at least 100-fold decreased compared with the potency (Figure 3A,B). These results suggested an allosteric binding mode of LMD-559 to both receptors.

GluVII:06 and TyrIII:08; the residues that bridge the minor and major binding pockets are essential for activation of CCR1 and CCR8 by small molecules

The potencies of the compounds shown in Figure 1B are critically dependent on GluVII:06 in CCR8 (Jensen *et al.*, 2007). LMD-559 displayed a similar >300-fold decreased potency for mutant receptors with Ala substitution of GluVII:06 in CCR8 and in CCR1 (Figure 4, Tables 1 and 2). In contrast, the endogenous ligands, CCL1 and CCL3, displayed unchanged high potency at these mutants of CCR8 and CCR1, respectively, indicating that Ala-substitution of GluVII:06 *per se* did not abolish activity (Figure 4, Tables 1 and 2). No effects were observed for Ala substitutions of residues in close proximity to GluVII:06: position VII:10/7.43 (Phe^{290} in CCR8 and Tyr^{291} in CCR1) and VII:03/7.36 (His^{283} in CCR8 and Gln^{284} in CCR1) located one helical turn above and below, supporting a direct role of GluVII:06 (Tables 1 and 2).

Position III:08/3.32 is a key interaction point for monoamines (Strader *et al.*, 1987) and for most non-peptides targeting CC-chemokine receptors (Berkhout *et al.*, 2003; Castonguay *et al.*, 2003; de Mendonca *et al.*, 2005; Maeda *et al.*, 2006; Vaidehi *et al.*, 2006; Jensen *et al.*, 2007). As observed for the CCR8-selective compounds in Figure 1B, the potency of LMD-559 also depended on TyrIII:08 in CCR1 and CCR8 as 133- and >394-fold decreased potency was observed for the TyrIII:08Ala mutant, respectively (Figure 5E,F), whereas the endogenous ligands were much less affected (6.6- and 19-fold decrease for CCL3 and CCL1, respectively) (Tables 1 and 2B).

Molecular mapping of LMD-559 in CCR8

Previous mapping of the CCR8-selective compounds (Figure 1B) suggested that the phenoxybenzyl 'right'-side moieties were located in the *minor* binding pocket – stabilized by aromatic residues in TM-I (TyrI:07/1.39 and PheI:11/1.43) and TM-II (PheII:17/2.57) – and that the chemically diverse 'left' side was located in the major binding pocket stabilized in a unique pattern depending on the chemical structure of each ligand (Jensen *et al.*, 2007). A similar dependency on TyrI:07, PheI:11 and PheII:17 was observed for LMD-559 in CCR8 with the most marked effect being obtained for the Ala substitution of TyrI:07 (Table 2A). As for the CCR8-selective agonists (Jensen *et al.*, 2007), the Ala substitution of Phe in II:13/2.53, III:07/3.31 and III:18/3.43 had no effect on potencies (Table 2A).

The area delimited by TM-III, IV and V in the 'upper' part of the *major* binding pocket contains several residues with putative tetrazol interaction properties. As tetrazols are considered as a carboxyl isostere (and potentially negatively charged), we initially focused on two positively charged lysines in position V:01/5.35 (Lys^{195}) and V:-02 (Lys^{193}), the only positively charged residues facing the binding pocket. Of these, LysV:01 is most conserved (50%) among endogenous chemokine receptors and known to interact with aplaviroc at CCR5 (Maeda *et al.*, 2006). However, Ala substitution of these Lys residues or the intervening TrpV:-01 (Trp^{194}) did not affect LMD-559 potency (Table B). The interface between TM-III and -IV contains two Tyr residues – which are also putative tetrazol interaction partners – in positions III:09/3.33 (Tyr^{114}) and IV:24/4.64 (Tyr^{172}). Accordingly, we observed a 44-fold decrease in potency for LMD-559 upon Ala substitution of TyrIII:09 (Figure 5A, Table 2B), compared with a selectively lower effect (between 3.7- and 25-fold decrease) for the CCR8-selective compounds (Figure 5B) (Jensen *et al.*, 2007). Importantly, TyrIV:24 turned out to be a completely selective hit for LMD-559, with a 40-fold decrease in potency upon Ala substitution, with no effect on the CCR8-selective compounds (Figure 5C,D, Table 2B), whereas Ala substitution of the residue lying above, SerIII:05/3.29 (Ser^{110}) had no effect (Table 2).

Table 1

Molecular interaction of CCL3, CCL5 and LMD-559 with CCR1 WT and mutations

			CCR1	CCL5 EC_{50} ± SEM (log)	EC_{50} (nM)	Fold	*n*	CCL3 EC_{50} ± SEM (log)	EC_{50} (nM)	Fold	(n)	LMD-559 EC_{50} ± SEM (log)	EC_{50} (nM)	Fold	*n*	Expression % of WT	*n*
A			CCR1 WT	−8.78 ± 0.09	1.6	1.0	42	−8.43 ± 0.04	3.7	1.0	(78)	−7.38 ± 0.10	42	1.0	14	100 ± 0.0	8
	Minor binding pocket	I:07	Y41A	−8.01 ± 0.10	9.9	6.0*	8	−8.44 ± 0.17	3.6	1.0	(10)	−6.77 ± 0.11	169	6.7**	6	52 ± 2.6	3
		I:11	F45A	−8.23 ± 0.63	5.9	3.6	3	−7.90 ± 0.04	13	3.4	(4)	−7.41 ± 0.18	39	0.94	4	52 ± 1.1	3
		II:18	P88A	−8.52 ± 0.16	3.0	1.8	3	−7.92 ± 0.12	12	3.3	(6)	−6.27 ± 0.04	533	13***	3	33 ± 9.3	3
		II:20	W90A	−7.13 ± 0.17	74	45*	3	−8.75 ± 0.09	1.8	0.48	(6)	−5.94 ± 0.18	1148	28***	4	112 ± 7.8	3
		II:20	W90Q	<−6	1000	>609***	3	−7.47 ± 0.09	34	9.3**	(3)	−6.05 ± 0.11	882	21***	3	112 ± 1.8	3
		II:24	K94A	−8.90 ± 0.06	1.3	0.77	3	−8.75 ± 0.12	1.8	0.48	(8)	−6.32 ± 0.18	482	12***	4	110 ± 9.8	3
		III:07	F112A	−8.76 ± 0.02	1.7	1.1	3	−8.47 ± 0.15	3.4	0.92	(7)	−7.39 ± 0.12	41	1.0	3	95 ± 3.0	3
		VII:03	Q284A	−8.71 ± 0.19	1.2	1.9	3	−8.24 ± 0.21	5.8	3.6	(3)	−8.01 ± 0.06	7.9	0.19	3	101 ± 5.6	3
		VII:10	Y291A	−7.71 ± 0.33	19	12**	3	−8.64 ± 0.21	2.3	0.62	(9)	−7.88 ± 0.18	13	0.32	5	87 ± 7.8	3
B	Major binding pocket	III:05	S110A	−8.49 ± 0.12	3.2	2.0	3	−8.73 ± 0.10	1.9	0.50	(5)	−7.77 ± 0.22	17	0.41	4	105 ± 9.3	3
		III:08	Y113A	−8.04 ± 0.14	9.0	5.5***	13	−8.80 ± 0.10	1.6	0.43	(21)	−5.25 ± 0.19	5630	135***	4	98 ± 4.7	3
		III:09	Y114A	−8.63 ± 0.13	2.4	1.4	4	−9.00 ± 0.14	1.0	0.27	(9)	−7.23 ± 0.11	59	1.4	4	105 ± 20	3
		V:-01	W195A	−8.32 ± 0.06	4.8	2.9	3	−7.56 ± 0.20	27	7.4*	(4)	−6.75 ± 0.16	176	4.2	3	116 ± 5.4	3
		V:01	K196A	−8.69 ± 0.19	2.0	1.2	3	−7.98 ± 0.02	11	2.9	(6)	−6.91 ± 0.03	124	3.0	4	104 ± 3.3	3
		V:11	F206A	−9.20 ± 0.30	0.63	0.38	4	−8.43 ± 0.16	3.7	1.0	(7)	−7.31 ± 0.10	49	1.2	4	92 ± 4.6	3
		VI:09	F248A	−8.44 ± 0.10	3.6	2.2	3	−7.96 ± 0.05	11	3.0	(8)	<−6	<1000	>24***	4	71 ± 4.3	3
		VI:13	W252A	−8.09 ± 0.19	8.2	5.0**	10	−8.44 ± 0.11	3.6	0.98	(20)	−6.90 ± 0.02	127	3.1	7	48 ± 5.5	3
		VI:16	Y255A	−7.89 ± 0.06	13	7.9***	12	−8.61 ± 0.15	2.5	0.67	(16)	−6.16 ± 0.06	697	17***	3	75 ± 3.4	3
		VII:06	E287A	−7.48 ± 0.12	33	20**	3	−8.38 ± 0.20	4.2	1.1	(6)	NA		NA***	3	115 ± 12	3
C	Extracell.	ECL-2B	F187A	−7.52 ± 0.32	30	18**	3	<−6	1000	>272***	(2)	−6.28 ± 0.12	525	13***	3	86 ± 5.2	3
		N-term	Δ4	−9.15 ± 0.26	0.71	0.43	4	−8.39 ± 0.23	4.1	1.1	(4)	−7.33 ± 0.14	46	1.1	4	106 ± 8.2	3
		N-term	Δ14	−7.62 ± 0.14	24	15**	4	−7.29 ± 0.21	51	14*	(4)	−7.36 ± 0.12	43	1.0	4	66 ± 2.8	3
		N-term	Δ23	NA		NA***	4	NA		NA***	(4)	−7.32 ± 0.16	48	1.2	4	64 ± 5.6	3

The different receptor constructs were transiently transfected in COS-7 cells, and the ligand-mediated activation was tested using IP_3 accumulation. The potencies are shown as as $LogEC_{50}$ (means ± SEM) and mean EC_{50}, with the number of experiments (*n*). Potency ratios of a given ligand between mutant and WT receptors is shown as 'fold'. $^*P < 0.02$, $^{**}P < 0.005$, $^{***}P < 0.001$; significantly different from WT values; two-sample *t*-test. Yellow background indicates 5- to 10-fold shift, orange background 10- to 50 –fold shift and red background >50-fold shift. In addition, the expression level, determined by an ELISA-based method, is provided for all mutations.

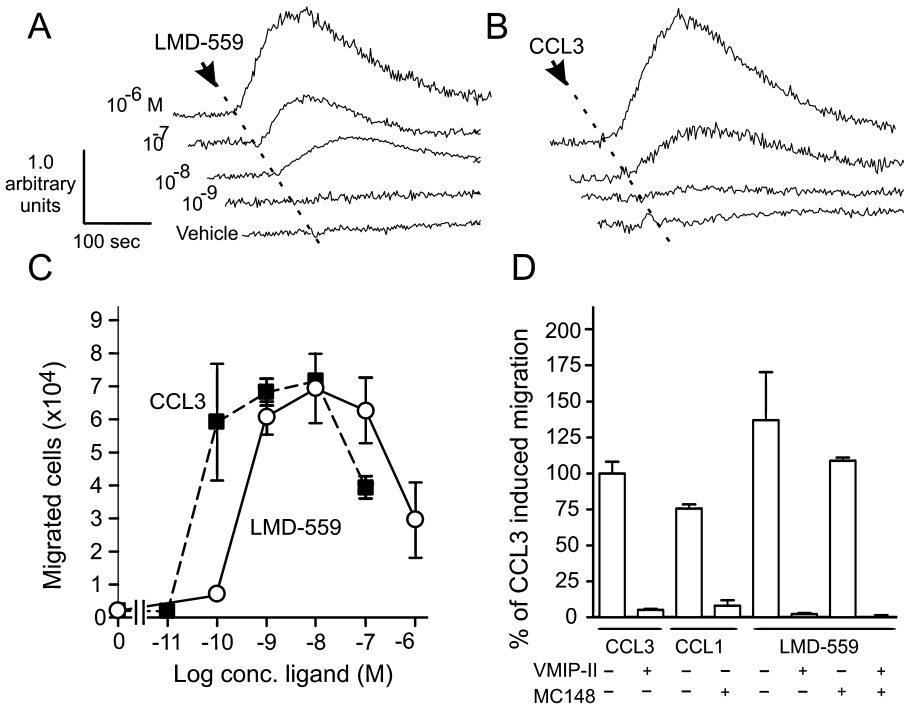

Figure 2

LMD-559 induced calcium release and chemotaxis via CCR1 activation. (A,B) Representative calcium release experiments performed in CCR1 stably transfected CHO cells using LMD-559 (A) and CCL3 as a positive control (B). (C) Representative chemotaxis experiments performed in THP-1 cells with CCL3 and LMD-559. (D) Effect on LMD-559 (100 nM) induced chemotaxis in cells pre-incubated with 100 nM of the CCR1 antagonist vMIP-II or 100 nM of the CCR8 antagonist MC148. CCL3 and CCL1 were included in the study at 10 nM each (n = 3).

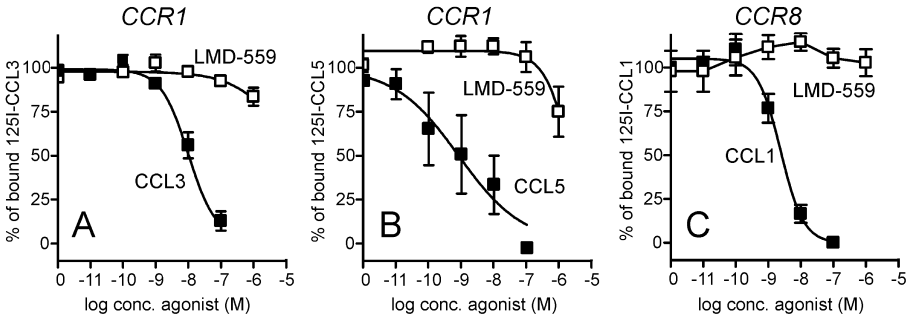

Figure 3

LMD-559 does not compete with endogenous chemokines for binding to CCR1 and CCR8. Heterologous binding experiments were performed in transiently transfected COS-7 cells. (A–C) Homologous and heterologous binding of CCL3 to CCR1 (A), CCL5 to CCR1 (B) and CCL1 to CCR8 (C). The curves have been normalized against homologous binding on the given receptor (n = 4).

In TM:VI, Ala substitution of PheVI:16 (Phe^{254}) – located at the same horizontal level as TyrIII:08 –resulted in a 6.4-fold decrease in potency of LMD-559, whereas CCL1 potency was unaffected. In contrast, the Ala substitution of TrpVI:13/6.48 (Trp^{251}) one helical turn below had a much lesser effect and no effect was observed for the Ala substitution of residues one and two helical turns above: LeuVI:20/6.55 (Leu^{258}) and SerVI:24/6.59 (Ser^{262}) (Table 2B). Together, these data, summarized in Figure 6A, suggest that the phenoxybenzyl moiety – common for all compounds in Figure 1 – is located in the *minor* binding pocket in CCR8, and that the phenyl-tetrazol-moiety (unique for LMD-559) is located in the 'upper' part of the major binding pocket in the interface between TM-III and IV.

Molecular modelling supports the mutational studies in CCR8

Molecular modelling with CCR8 built over the crystal structure of CXCR4 clearly supported the binding mode predicted from the mutational studies. Thus, the phenoxy-tetrazol

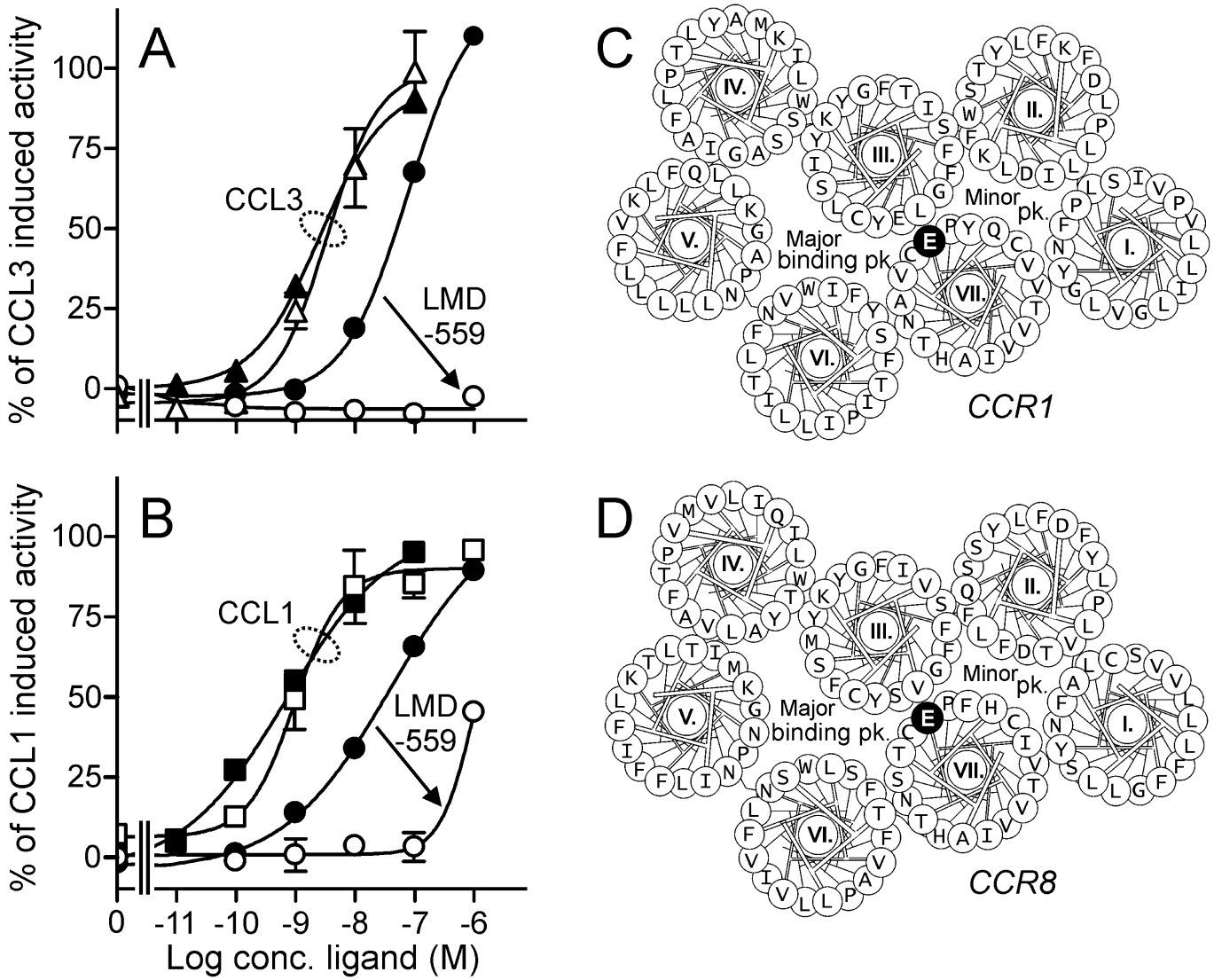

Figure 4

GluVII:06 is essential for activation by a non-peptide agonist, but not for activation by chemokines. IP_3 accumulation experiments were performed in transiently transfected COS-7 cells. (A) Dose–response curves for CCL3 and LMD-559 at wild-type CCR1 (filled symbols) and the mutant CCR1-[E287A] (open symbols). (B) Dose–response curves for CCL1 and LMD-559 at wild-type CCR8 (filled symbols) and the mutant CCR8-[E286A]. Note that the activity of chemokines was unchanged at the mutant receptors in contrast to the marked loss of activity for LMD-559. (C,D) Helical wheel models of CCR1 (C) and CCR8 (D) with the residues mutated in the present study highlighted in grey. The conserved GluVII:06 is highlighted in black. The minor and major binding pockets are indicated (n = 3–6).

moiety was identified in the major binding pocket of CCR8 with the tetrazol group stabilized by aromatic and hydrophilic interactions with TyrIII:09 and TyrIV:24 (with maximum distance of 3.1 Å) and the phenyl group stabilized by PheVI:16 (Figure 6B,C). As predicted, a charge–charge interaction was identified in the bridge area between the major and minor binding pocket between GluVII:06 and the amine in the piperidine ring. Of the three identified aromatic residues in the minor binding pocket (TyrI:07, PheI:11 and Phe II:17), the most superficial and most important for small molecule activation (TyrI:07) was located closest to LMD-559 (Figure 6).

TM-II plays a crucial role in activity of LMD-559 at CCR1, but not at CCR8

Notable structural differences are found between CCR1 and CCR8 with respect to TM-II. Thus, 85% of all chemokine receptors (incl. CCR1) contain a Trp in II:20/2.60 that is essential for small molecule action in several cases (Seibert *et al.*, 2006). This is also the case in CCR1, where a 28-fold decrease in LMD-559 potency occurred after Ala substitution of TrpII:20 (Figure 7A), whereas CCL3 was unaffected (Table 1A). CCR8, however, has a Gln in II:20 (Gln^{91}), that was unimportant as neither Ala nor the CCR1-like Trp sub-

Table 2

Molecular interaction of CCL1 and LMD-559 with CCR8 wt and mutations

				CCL1				LMD-559				Expression	
			CCR8	EC_{50} ± SEM (log)	EC_{50} (nM)	Fold	*n*	EC_{50} ± SEM (log)	EC_{50} (nM)	Fold	*n*	% of WT	*n*
A			CCR8 wt	–9.16 ± 0.11	0.70	1.0	37	–7.48 ± 0.12	33	1.0	11	100 ± 0	9
	Minor binding pocket	I:07	Y42A	–9.17 ± 0.11	0.68	1.0	3	–6.72 ± 0.22	192	5.8*	2	72 ± 9.6	3
		I:11	F46A	–9.01 ± 0.11	0.97	1.4	4	–6.94 ± 0.10	115	3.5	3	75 ± 3.1	3
		II:13	F84A	–8.75 ± 0.21	1.80	2.6	3	–7.71 ± 0.14	20	0.60	4	30 ± 9.1	3
		II:17	F88A	–8.66 ± 0.13	2.2	3.2	3	–7.16 ± 0.03	69	2.1	3	8.7 ± 2.2	3
		II:18	P89A	<–7	>100	>143***	3	–7.31 ± 0.29	50	1.5	3	46 ± 4.1	3
		II:20	Q91A	–8.87 ± 0.19	1.4	2.0	3	–7.95 ± 0.28	11.3	0.34	3	53 ± 0.45	3
		II:20	Q91W	–7.87 ± 0.19	13	19*	3	–6.89 ± 0.31	130	3.9	3	17 ± 7.7	3
		III:07	F112A	–9.36 ± 0.24	0.44	0.63	3	–7.51 ± 0.08	31	0.94	4	90 ± 7.6	3
		III:18	F123A	–9.61 ± 0.02	0.25	0.35	3	–7.66 ± 0.05	22	0.66	3	19 ± 3.3	3
		VII:03	H283A	–8.91 ± 0.34	1.24	1.8	3	–7.25 ± 0.10	56	1.7	3	60 ± 8.6	3
		VII:10	F290A	–8.35 ± 0.30	4.5	6.4*	4	–7.19 ± 0.11	64	1.9	3	27 ± 12	3
B	Major binding pocket	III:05	S110A	–9.19 ± 0.24	0.65	1.3	4	–7.77 ± 0.22	17	0.51	5	36 ± 9.2	3
		III:08	Y113A	–7.88 ± 0.05	13	19*	3	<–5	>10 000	>394***	3	21 ± 10	3
		III:09	Y114A	–9.03 ± 0.10	0.94	1.3	4	–5.84 ± 0.43	1 454	44***	3	17 ± 9.4	2
		IV:24	Y172A	–8.07 ± 0.09	8.5	12*	3	–5.87 ± 0.39	1 338	40***	3	8.6 ± 1.4	3
		V:-02	K193A	–7.87 ± 0.09	13	19**	3	–7.75 ± 0.10	18	0.53	4	35 ± 13	3
		V:-01	W194A	–9.34 ± 0.31	0.46	0.66	4	–7.83 ± 0.46	15	0.44	4	68 ± 17	3
		V:01	K195A	–9.41 ± 0.14	0.39	0.56	3	–7.65 ± 0.05	22	0.67	3	19 ± 12	3
		VI:13	W251A	–8.18 ± 0.79	6.6	9.4**	3	–7.08 ± 0.53	83	2.5	3	15 ± 4.1	2
		VI:16	F254A	–9.07 ± 0.22	0.85	1.2	3	–6.67 ± 0.09	213	6.4***	3	27 ± 3.6	3
		VI:20	L258A	–8.58 ± 0.14	2.64	3.8	3	–7.09 ± 0.14	82	2.5	3	91 ± 21	3
		VI:24	S262A	–9.21 ± 0.14	0.62	0.9	3	–7.44 ± 0.08	36	1.1	4	38 ± 16	3
		VII:06	E286A	–8.65 ± 0.39	2.2	3.2	3	<–5	>10 000	>394***	3	27 ± 10	3
		VII:09	S289A	–9.06 ± 0.34	0.86	1.2	3	–7.16 ± 0.05	69	2.1	3	97 ± 11	3
C	Extracellular regions	ECL-2	Y184A	–7.85 ± 0.05	14.0	20***	5	–8.02 ± 0.32	9.5	0.29	3	94 ± 2.7	3
		ECL-2	Y184A-F186A-Y187A	NA		NA***	3	–8.52 ± 0.25	3.0	0.09**	3	85 ± 20	3
		ECL-2	F186A	–8.33 ± 0.21	4.7	6.7***	7	–7.55 ± 0.57	28	0.84	3	136 ± 13	3
		ECL-2	Y187A	–9.03 ± 0.19	0.93	1.3	7	–8.55 ± 0.39	2.8	0.09**	3	73 ± 15	3
		N-term	Δ4	–9.07 ± 0.25	0.84	1.2	6	–7.55 ± 0.34	28	0.86	3	100 ± 16	3
		N-term	Δ12	–8.64 ± 0.22	2.3	3.3	5	–7.72 ± 0.17	19	0.57	3	32 ± 7.3	3
		N-term	Δ24	NA		NA***	4	–7.65 ± 0.26	22	0.68	3	35 ± 5.4	3

The different receptor constructs were transiently transfected in COS-7 cells, and the ligand-mediated activation was tested using IP_3 accumulation.. The potencies are shown as as $LogEC_{50}$ (means ± SEM) and mean EC_{50}, with the number of experiments (*n*). Potency ratios of a given ligand between mutant and WT receptors is shown as 'fold'. $^*P < 0.02$, $^{**}P < 0.005$, $^{***}P < 0.001$; significantly different from WT values; two-sample *t*-test. Yellow background indicates 5- to 10-fold shift, orange background 10- to 50-fold shift and red background >50-fold shift. In addition, the expression level, determined by an ELISA-based method, is provided for all mutations.

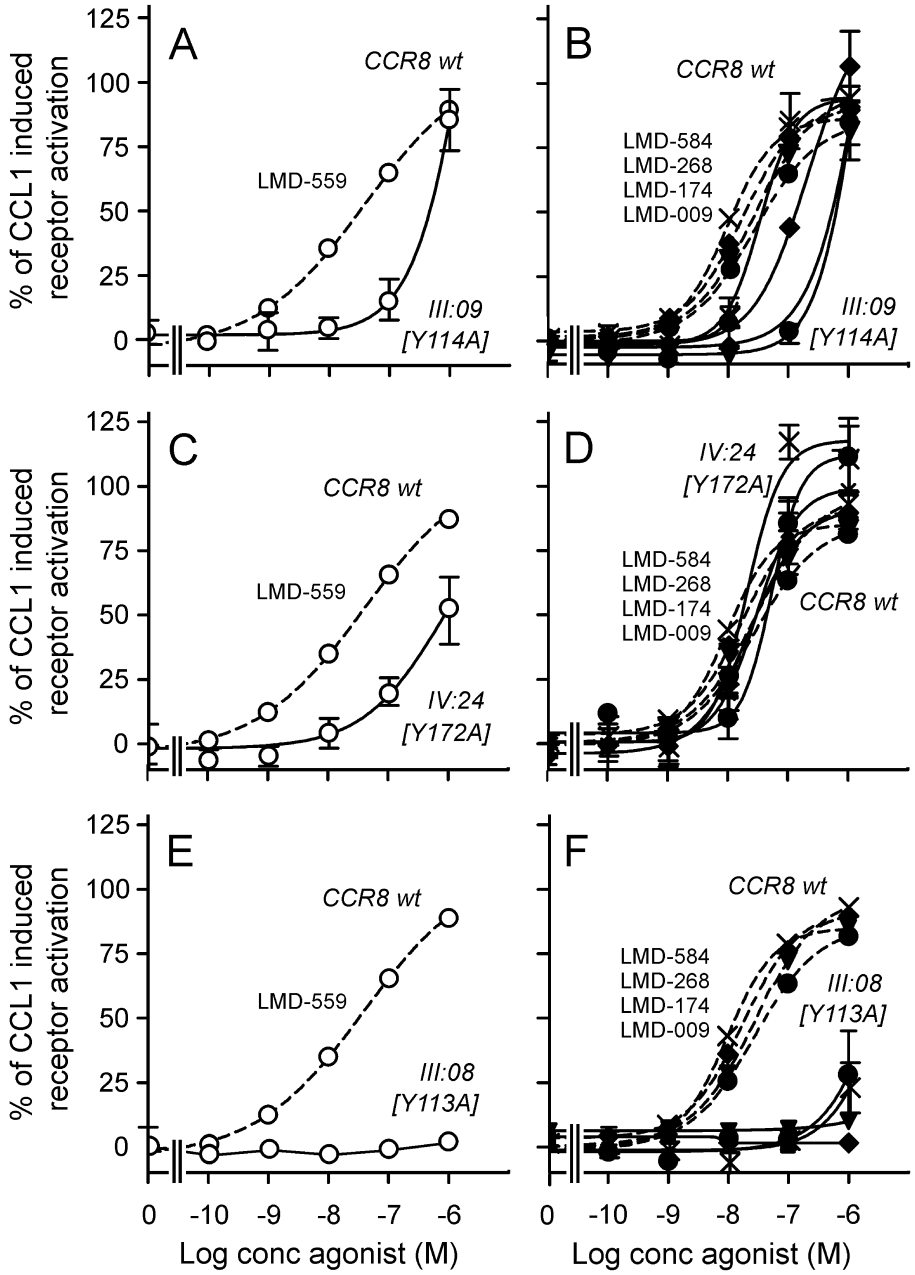

Figure 5

Activity of LMD-559 is dependent on aromatic residues in the major binding pocket in CCR8. IP_3 accumulation experiments were performed in transiently transfected COS-7 cells. Dose–response curves of the dually active LMD-559 (A,C,E) and the CCR8-selective compounds (B,D,F) on wild-type CCR8 (wt; dashed lines) and various CCR8 mutants (solid lines). All curves were normalized against CCL1 induced activation on each receptor. (A,C,E) Dose–response curves of LMD-559 on [Y114A]-CCR8 (A), [Y172A]-CCR8 (C) and [Y113A]-CCR8 (E). (B,D,F) Dose–response curves of LMD-174, -009, -584 and -268 on [Y114A]-CCR8 (B), [Y172A]-CCR8 (D) and [Y113A]-CCR8 (F) (n = 3–4).

stitution (Table 2A) had any effect on LMD-559 binding. In contrast, a Gln introduced at II:20 in CCR1 had the same marked effect as Ala, indicating that proper action of LMD-559 in CCR1 requires a Trp in II:20 (Table 1A). Position II:24/2.64 in CCR1 holds a Lys that points right into the minor binding pocket – one helical turn above TrpII:20. Importantly, Ala substitution of LysII:24 resulted in a 12-fold decrease in LMD-559 potency (Figure 7B), whereas the endogenous ligands were unaffected (Table 1B).

A further corroboration of the importance of TM-II in CCR1 was provided by a helix-distortion, straightening of the proline kink in position II:18/2.58. Thus, whereas a 13-fold decrease for LMD-559 potency was observed for the Ala substitution of Pro^{88} in CCR1 (Figure 7C, Table 1A), no change was observed for LMD-559 by the similar substitution in CCR8 (Figure 7C, Table 1). Finally, of the three aromatic residues: TyrI:07 (Tyr^{41}), PheIII:07 (Phe^{112}) and TyrVII:10 (Tyr^{291}) confining the *minor* binding pocket in CCR1, only TyrI:07

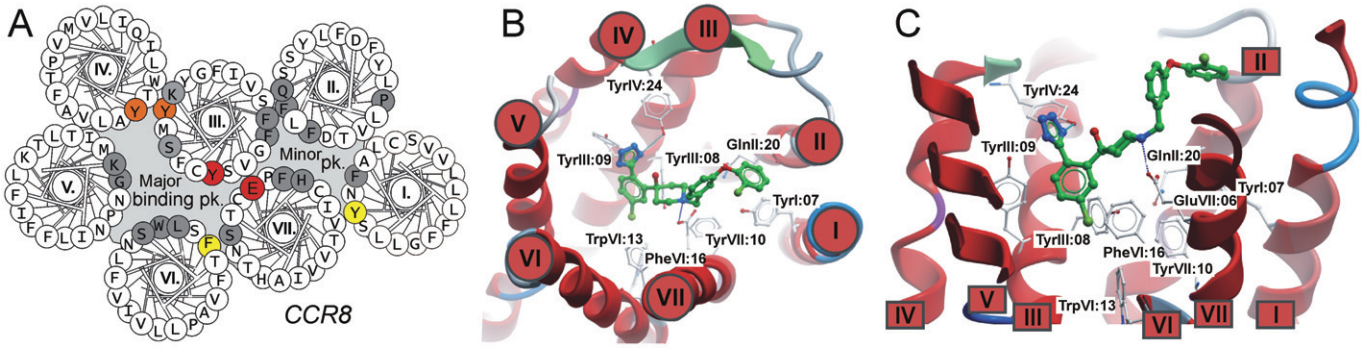

Figure 6

Molecular model of LMD-559 binding in CCR8. (A) Effect of the Ala substitution of residues in the minor and major binding pocket of CCR8. The colour code indicates the effect on potency of LMD-559 for a given mutation relative to wild-type CCR8 activation. Grey residues indicate <5-fold decrease in potency, yellow indicates 5- to 25-fold decrease, orange indicates 25- to 100-fold decrease and red indicates >100-fold decrease. B and C depict the molecular model of LMD-559 (green stick) binding in CCR8 using the CXCR4 crystal structure as template. The model is shown from the extracellular side (B) and from the side corresponding to TM-VI and -VII (both partly removed) (C). For simplicity, the extracellular receptor regions are not shown.

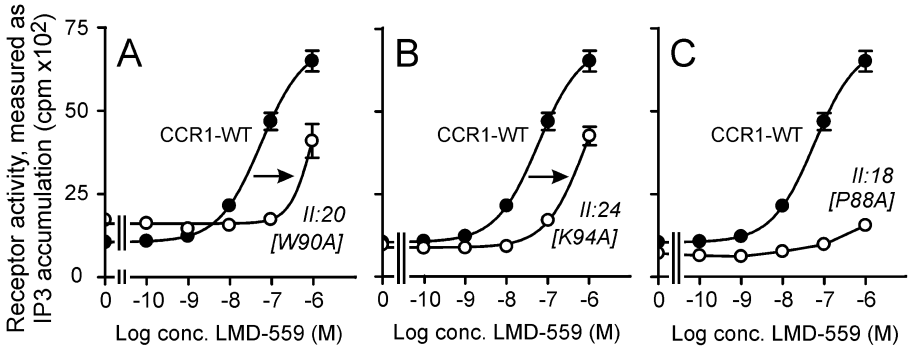

Figure 7

Activation of CCR1 by LMD-559 depends on residues in TM-II. The IP_3 accumulation experiments were performed in transiently transfected COS-7 cells and are presented as the mean of at least three separate experiments. (A–C) Dose–response curves of LMD-559 on wild-type CCR1 (WT) or mutant receptor. [W90A]- (A), [K94A]- (B) and [P88A]-CCR1 (C) (n = 3–4).

was important for LMD-559 as an eightfold decrease in potency was observed upon Ala substitution (Table 1A).

Mutational mapping of LMD-559 in the major binding pocket of CCR1

Although the *major* binding pockets of CCR1 and CCR8 are very similar, they differ with respect to the identified tetrazol interaction residue TyrIV:24 in CCR8, as CCR1 contains a Ser in IV:24 (Ser^{172}). However, the neighbouring TyrIII:09 is conserved, and in contrast to its important role in CCR8 (Figure 5A), no change was observed upon the Ala substitution of TyrIII:09, or for the SerIII:05 (Ser^{110}) lying above in CCR1 (Table 1B). In TM-V, LMD-559 was unaffected by Ala substitution of the two aromatic residues PheV:11/5.45 (Phe^{206}) and TrpV:-01 (Trp^{195}), and of the Lys in V:01 (Lys^{196}) (Table 1B). In contrast, Ala substitutions of the aromatic residues in TM-VI had some effect on LMD-559 potency with >24-fold decrease for PheVI:09/6.44 (Phe^{248}), and 17-fold decrease for TyrVI:16 (Tyr^{255}), whereas CCL3 potency was unaffected (Table 1B). Thus, in summary, several aromatic residues facing into the major binding pocket, especially the 'lower' part, delimited by TM-III, VI, and VII were identified as important for LMD-559 activity.

Importantly, all experiments were performed along with a variant of LMD-559 (LMD-051), that contained a methoxy group instead of a chloride group in the phenoxybenzyl moiety and, in this respect, was a closer structural analogue of the previously tested CCR8-specific agonists (Figure 1B). LMD-051 shared similar interaction-profiles with LMD-559 (data not shown) but in general displayed approximately 10-fold lower potency than LMD-559 for CCR1. Consequently, LMD-559 was chosen for the mutational studies.

Molecular modelling supports the mutational studies in CCR1

As with CCR8, molecular modelling of CCR1 clearly supported the binding mode predicted from the mutational studies summarized in Figure 8A, as the phenyl-tetrazol

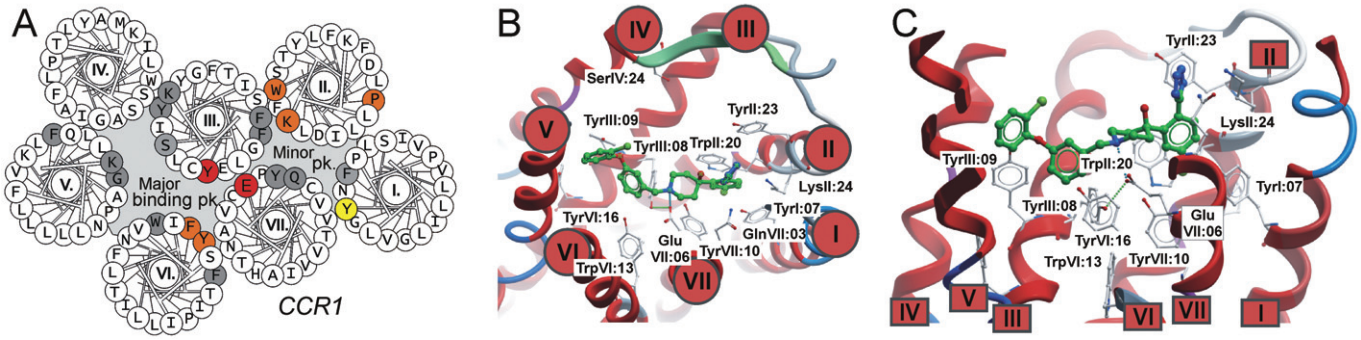

Figure 8

Molecular model of LMD-559 binding to CCR1. (A) Effect of the Ala substitution of residues in the minor and major binding pocket of CCR1. The colour code indicates the effect on potency of LMD-559 for a given mutation relative to wild-type CCR1 activation. Grey residues indicate <5-fold decrease in potency, yellow indicates 5- to 25-fold decrease, orange indicates 25- to 100-fold decrease and red indicates >100-fold decrease. B and C depict the molecular model of LMD-559 binding in CCR1, using the CXCR4 crystal structure as template. LMD-559 is depicted as a green stick model. The molecular interactions are shown from the extracellular side (B) and from the side (C). For simplicity, the extracellular receptor regions have been omitted.

moiety was localized in the *minor* binding pocket of CCR1 with the tetrazol group stabilized by charge–charge interactions with LysII:24 (distance of 3.1 Å) and the phenyl group interacting with TrpII:20 (Figure 8B,C). In addition, TyrII:23/6.23 was identified as being part of the binding pocket for LMD-559. As in CCR8, GluVII:06 was identified as anchor for the positively charged amine in the piperidine ring. The phenoxybenzyl moiety ('right' side) was not only localized in the major binding pocket interacting with and stabilized by TyrIII:08 and TyrVI:16 in particular but also influenced by the deeper located TrpVI:13 in a more indirect stabilizing manner (Figure 8B,C).

Importance of extracellular domains in CCR1 and CCR8

The observed differences in binding mode of LMD-559 in CCR1 and CCR8 prompted us to explore the contribution of the ECL-2 – a region with increasing importance for rhodopsin-like 7TM receptors (Peeters *et al.*, 2011). First, the conserved disulphide bridge between TM-III (CysIII:01/3.25) and ECL-2 was disrupted by an Ala substitution of CysIII:01. However, no agonists were able to activate these receptors, and ELISA-based expression analyses revealed low surface expression (<20% of WT receptors; data not shown). We therefore focused on aromatic residues in ECL-2B, given the participation of ECL-2B in ligand binding (Cherezov *et al.*, 2007; Rosenbaum *et al.*, 2007; Jaakola *et al.*, 2008; Wu *et al.*, 2010). In CCR1, only one such residue is found (Phe^{187}, located four residues after Cys^{183}), and Ala substitution here resulted in a robust decrease in potency of LMD-559 (Figure 9A). CCL3 and -5 were also affected with 18-fold decrease in the potency of CCL5 and 272-fold for CCL3 (Figure 9B, Table 1C), whereas the receptor surface expression level was comparable to WT receptors (Table 1C). A completely different picture emerged with CCR8 which contains three aromatic residues in ECL-2B (Tyr^{184}, Phe^{186} and Tyr^{187}, located in *i*+1, *i*+3 and *i*+4), as substitution by Ala, singly or together, of these residues did not decrease potency of LMD-559 (Figure 9D, Table 2C). In fact, a potency increase was observed in all mutations, with up to 11-fold increase in the triple-Ala substitution. Importantly, the opposite effect was observed for CCL1 with virtually no CCL1-mediated activation in the triple mutation (Figure 9D, Table 2C). Interestingly, the potency of LMD-559 was increased together with a marked decrease in efficacy despite unaltered receptor surface expression, indicating that the ECL-2 contributed to the stabilization of the receptor–LMD-559 complex in an active conformation, without directly contributing to the binding site of LMD-559.

Chemokine receptor N-termini are essential for chemokine, but not small molecule, binding (Schwarz and Wells, 2002; Rosenkilde and Schwartz, 2006; Allen *et al.*, 2007; Jensen and Rosenkilde, 2009). Given the differential impact of ECL-2B (Figure 9), we explored the role of the N-terminus for LMD-559 in CCR1 and CCR8. As for the previously characterized CCR8-selective compounds (Figure 1B) (Jensen *et al.*, 2007) and in contrast to the chemokine-mediated activation that declined as expected, we observed no change in potencies of the tetrazol-containing compounds for consecutive N-terminal truncations (Tables 1C and 2C), indicating that the N-termini were indeed important for chemokine, but not for small molecule, activation.

Molecular modelling of ECL-2

Recent crystal structures of class A 7TMs have disclosed that ECLs – in particular ECL-2B – may participate in ligand binding (Palczewski *et al.*, 2000; Cherezov *et al.*, 2007; Jaakola *et al.*, 2008; Warne *et al.*, 2008; Nygaard *et al.*, 2009). The observed effect of ECL-2B in CCR1 was indeed supported by the modelling studies. Thus, based on the crystal structure of CXCR4, ECL-2B in CCR1 was arranged in a β-sheet with Phe^{187} identified as a direct interaction partner for the phenoxybenzyl moiety in LMD-559 localized in the *major binding pocket*, whereby Phe^{187} together with TyrIII:08, TyrIII:09, TyrVI:16 and to a lesser extent the deeper located TrpVI:13 constituted the aromatic binding pocket for this part of LMD-

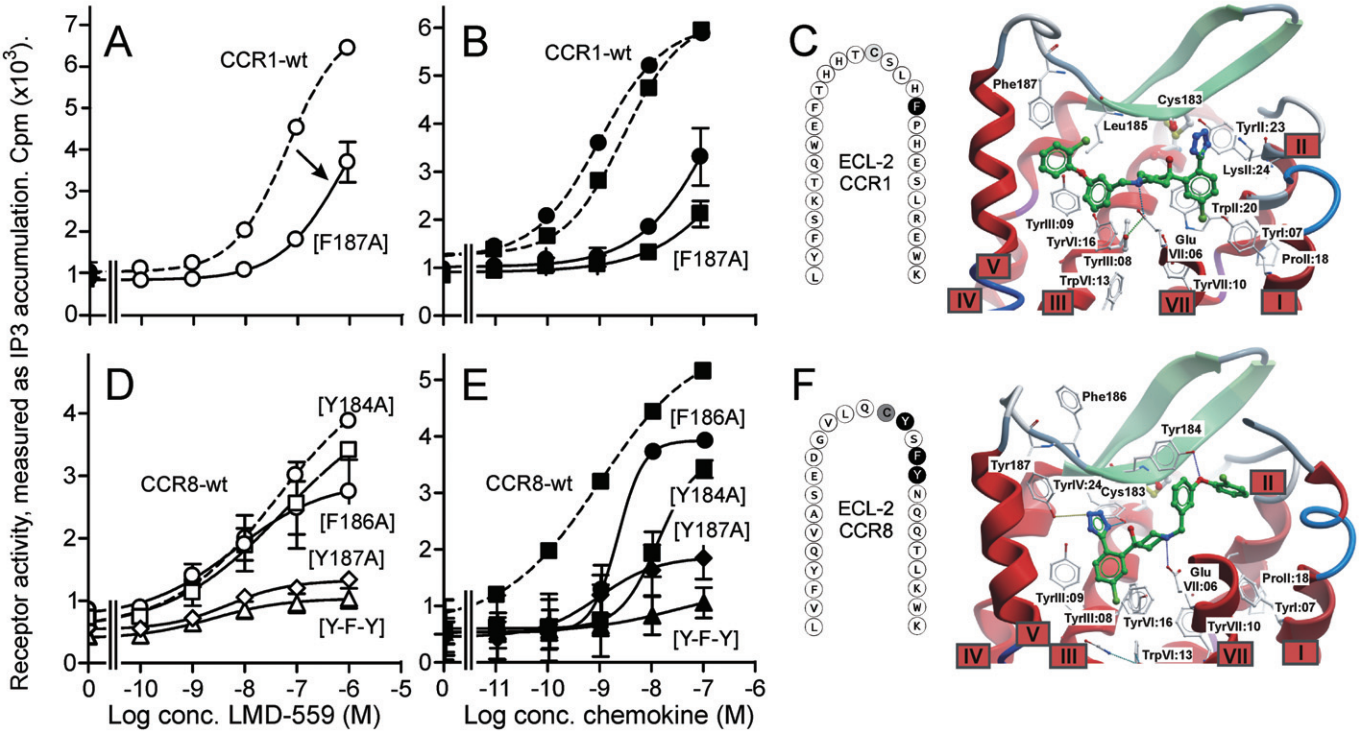

Figure 9

Influence of ECL-2 for the activity of LMD-559. (A,B,D,E) IP_3 accumulation experiments performed in transiently transfected COS-7 cells and presented as the mean of at least three separate experiments. (A,D) Dose–response curves of LMD-559 on wild-type (wt; dashed lines) or mutant receptors (solid lines). (A) [F187A]-CCR1. (D) [Y184A]-CCR8, [F186A]-CCR8, [Y187A]-CCR8 and [Y184A,F186A,Y187A]-CCR8 (Y-F-Y). (B,E) Dose–response curves of endogenous ligands on wild-type (wt; dashed lines) or mutant receptors (solid lines). (B) [F187A]-CCR1 with CCL3 and CCL5. (E) CCL1 on [Y184A]-CCR8, [F186A]-CCR8, [Y187A]-CCR8 and [Y184A,F186A,Y187A]-CCR8. (C,F) Sequences of ECL-2 in CCR1 (C) and CCR8 (F) with the conserved Cys highlighted in grey and the included aromatic residues are highlighted in black. Adjacent are the molecular models of CCR1 and CCR8 shown similarly to the models in Figures 5 and 7, but including the ECL-2.

559 (Figure 9C). In CCR8, ECL-2B also formed a β-sheet with putative interaction between ECL-2B and LMD-559; however, in contrast to CCR1, the closest interaction was identified between Tyr^{184} (*i+1*) and the phenoxybenzyl moiety localized in the *minor binding pocket*. A secondary interaction – also of hydrophilic character – was identified between Tyr^{187} (*i+4*) and the tetrazol moiety localized in the *major binding pocket*.

Discussion

In the present study, we describe a dually active ligand that, in contrast to the structurally similar CCR8-selective agonists (Jensen *et al.*, 2007), activated CCR1 in addition to CCR8. Importantly, the ligand acted differentially at the molecular level in CCR1 and CCR8. In both receptors, a charge–charge interaction was formed between the positively charged quaternary amine (piperidine ring) and the negatively charged GluVII:06, but the rest was *mirrored*. Furthermore, we show that ECL-2B played different roles in CCR1 and CCR8. Thus, in CCR1, it stabilized LMD-559 in the *major binding pocket* and contributed to potency, whereas it mainly stabilized LMD-559 in the *minor binding pocket* of CCR8 and contributed to efficacy, but not potency – a phenomenon that inspires new thoughts about the molecular basis for potency as distinct from efficacy. Importantly, in our studies, several of the mutations resulted in low surface expression (<20% of WT expression), and as discussed previously, this may influence ligand potency and thus complicate the interpretation of the effects of a given mutation (Johnson *et al.*, 1979; Black and Leff, 1983; Bouvier *et al.*, 1988). However, in our system, the mutations that resulted in decreased surface expression showed unaltered potency of either endogenous or non-peptide ligands which thus could be a result of increased binding affinity of the given ligand.

A wealth of crystal structures for 7TM receptors

Recently, the crystal structure of CXCR4 was presented (Wu *et al.*, 2010). In contrast to the other structures, TM-I in CXCR4 is localized 'closer' to the pocket centre, presumably due to the chemokine-specific disulphide bridge between Cys residues in the N-terminus and in ECL-3. Furthermore, CXCR4 is the first crystal structure of a receptor with a Pro in II:18 (like CCR1 and CCR8), which creates a kink and thereby changes the coordinates and rotation of the exterior half of TM-II, resulting in position II:20 and II:24 pointing into the minor binding pocket (Wu *et al.*, 2010) (Figure 10). Analysis

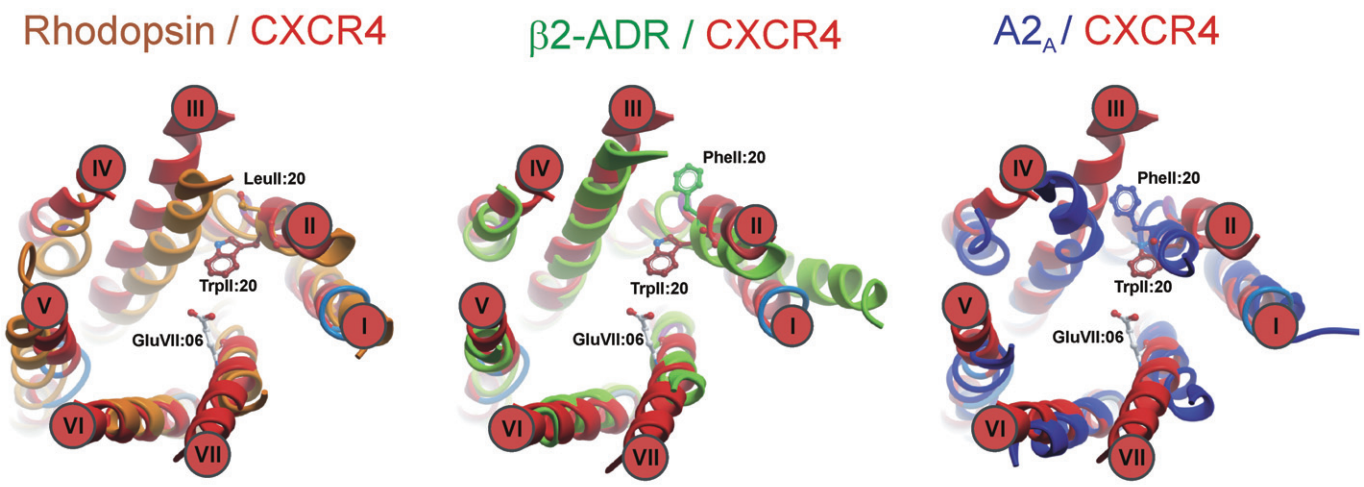

Figure 10

CXCR4 crystal structure compared with other available receptor crystal structures. CXCR4 (in red) is shown together with rhodopsin (orange), β_2-adrenoceptor (ADR) (green) and adenosine A_{2A} ($A2_A$) receptor (blue). In all three overlays, position II:20 is shown in sticks in order to emphasize the different orientations of TM-II in the different structures. The GluVII:06 (conserved in most chemokine receptors) is shown in sticks in the bridge area between the minor and major binding pockets.

of the main binding pocket in terms of depth, extension and division into a major and a minor binding pocket in the different crystal structures shows the clearest division in these two binding pockets for CXCR4, adenosine A_{2A} and β_2-adrenoceptors (Figure S3). Based on these observations, CXCR4 was chosen for the final modelling of LMD-559. However, before the release of the CXCR4 crystal structure, we used the β_2-adrenoceptor as the template (Figure S4) and importantly identified the same mirrored orientation of LMD-559 with the same key interaction points (Figure S4). Obviously, agonist docking into the CXCR4 crystal structure is associated with certain inaccuracies and assumptions, as the structure is in its inactive state, stabilized by antagonists. Thus, the structure does not elucidate the movements of the transmembrane segments, which are believed to follow agonist activation. Less is known about the extracellular parts of the activated receptor; although these highly flexible regions are similarly believed to undergo movements upon agonist binding (Peeters *et al.*, 2011).

General binding pattern of small molecule ligands in chemokine receptors

LMD-559 shares a similar pharmacophore with previously described non-peptide antagonists targeting CC-chemokine receptors in having an elongated structure with a more or less centrally located positively charged amine and flanking aromatic residues (Rosenkilde and Schwartz, 2006; Jensen and Rosenkilde, 2009). The conserved GluVII:06 serves as a corresponding perfect match, as described here for LMD-559 in CCR1 and CCR8, for the previously described CCR8-selective compounds (Jensen *et al.*, 2007), UCB-35625 in CCR1 (de Mendonca *et al.*, 2005) and several compounds targeting CCR2 and CCR5 (Mirzadegan *et al.*, 2000; Berkhout *et al.*, 2003; Castonguay *et al.*, 2003; Maeda *et al.*, 2006). In contrast to the characteristic promiscuity amongst most chemokines, non-peptides are usually more selective (Rosenkilde and Schwartz, 2006; Wells *et al.*, 2006). Exceptions however, are TAK-779 (CCR2, CCR5 and CXCR3 antagonist) (Baba *et al.*, 1999; Gao *et al.*, 2003) and UCB-35625 (dual-active CCR1 and CCR3 antagonist) (Sabroe *et al.*, 2000). Despite the existence of other dually specific small molecules, the observed *mirrored binding mode* in the present study has not been observed before.

Small molecule ligands for CCR1 – overlapping molecular interaction for agonists and antagonists

Intriguingly, the binding mode identified here for the small molecule *agonist* in CCR1 and CCR8 overlap considerably with those of small molecule *antagonists* in CC-chemokine receptors, such as BX471 and UCB-35625 in CCR1 (de Mendonca *et al.*, 2005; Vaidehi *et al.*, 2006), the spiropiperidines RS-50404393 and -102895, the Teijin compound and TAK-779 in CCR2 (Mirzadegan *et al.*, 2000; Berkhout *et al.*, 2003) and aplaviroc, TAK-779 and a series of pyrrolidine and acyclic compounds in CCR5 (Castonguay *et al.*, 2003; Maeda *et al.*, 2006). This is not surprising given the similar pharmacophores. It is however interesting, that despite roughly overlapping binding sites, these compounds display opposite pharmacology (being *agonists* and *antagonist*, respectively). In turn, this indicates that the key anchor points for different ligand classes may very well overlap, and that the final efficacy depends on the final conformational constraining of a certain receptor population (Schwartz and Rosenkilde, 1996). Recently, a different class of small molecule agonists for CCR1 was presented, acting as dual allosteric agonists that enhanced the binding of CCL3, but not CCL5 (Jensen *et al.*, 2008). Binding of LMD-559 partly overlapped with these

compounds, as it also anchored to GluVII:06. However, despite the partial overlap of binding sites for LMD-559 and CCL5 in, for instance, TM-II, -VI and -VII of CCR1, LMD-559 displaced CCL5 with very low affinity in competition binding, suggesting an overall allosteric binding mode of LMD-559.

Importance of TM-II for small molecule binding in CCR1, but not in CCR8

The majority of studies concerning 7TM receptor activation have focused on the major binding pocket as many residues facing this pocket are essential for the activation process. Nevertheless, the minor binding pocket – illustrated in Figure S3 – and in particular TM-II also plays a role for these processes in several cases (Benned-Jensen and Rosenkilde, 2009; Rosenkilde *et al.*, 2010). In CCR2 and CCR5 for instance, mutations in the TXP motif influence ligand-induced, as well as constitutive activity (Govaerts *et al.*, 2001; Arias *et al.*, 2003). Moreover, a study from 1994 indicated an essential role of TM-II for the interchange between different receptor conformations, as Ala substitutions of residues facing the minor binding pocket resulted in a conformational constraining of the NK_1 receptor (Rosenkilde *et al.*, 1994). In the present study, we observed that residues in the top of TM-II in CCR1 (TrpII:20 and LysII:24) were important for LMD-559, but not CCL3, indicating a direct interaction with LMD-559, as supported by the modelling studies. The impaired activity upon substituting ProII:18 to Ala in CCR1, thereby straightening TM-II, also supported this.

Position II:20 – a ligand-binding and activity switch in 7TM receptors

Position II:20 is located superficial to the Pro in TM-II and is, directly or indirectly, involved in ligand binding and constitutive activity in several 7TM receptors (Benned-Jensen and Rosenkilde, 2009; Rosenkilde *et al.*, 2010). In brief, a residue of either aromatic or aliphatic nature is found in this position (Mirzadegan *et al.*, 2003). Thus, 85% of chemokine receptors, inclusive of CCR1, but not CCR8, contain a Trp in II:20, compared with ~9% of non-chemokine class A receptors. Importantly, earlier findings in CCR2 and CCR5 suggest a direct interaction with hydrophobic parts of various non-peptide antagonists with the indole ring in TrpII:20 (Tsamis *et al.*, 2003; Maeda *et al.*, 2006; Hall *et al.*, 2009) in accordance with our findings in CCR1. Recently, a more indirect role of II:20 was presented for the orphan Epstein–Barr virus-induced receptor 2 (EBI2 or GPR183), as a positive charge in this position was necessary for maintaining high constitutive activity (Benned-Jensen and Rosenkilde, 2008; 2009).

Involvement of the extracellular parts in ligand binding – influence on potency and/or efficacy

In general, receptor N-termini and to a variable degree extracellular loops are important for chemokine binding (Allen *et al.*, 2007). In contrast, small molecule ligands for chemokine receptors bind more deeply in an allosteric binding mode (Wells *et al.*, 2006; Allen *et al.*, 2007). X-ray structures of at least three receptors indicate that ECL-2 participates directly in ligand binding (Figure S5) through aromatic residues located in the vicinity of the conserved Cys residue, in ECL-2B. These aromatic residues are also conserved in chemokine receptors, and our finding is thus in good agreement with previous observations. The effect on efficacy, but not potency of LMD-559 in CCR8, combined with the observation that ECL-2B mainly interacts with LMD-559 in the *minor binding pocket* in CCR8 indicates that this part of the main binding pocket may be more important for conformational constraining and maintenance of active receptor conformations (factors that contribute to ligand efficacy), than for constituting the binding site of LMD-559 (contributing to ligand potency). This is indeed supported by the rather superficial localization of LMD-559 in the *minor binding pocket* of CCR8. In other words, that the minor binding pocket and the stabilization by ECL-2B in CCR8 is important for ligand efficacy, whereas the potency (determined by the actual binding site) depends more upon ligand interaction in the major binding pocket. These observations clearly expand and diversify our knowledge about the impact of ECL-2 for proper receptor function.

In summary, we describe a dually active potent compound that interacts differently with homologous receptors – a finding that may have considerable importance for drug discovery as it illustrates the complexity of ligand interaction and the phenomenon of bitopic ligands. The suggested mirrored or reversed binding mode in CCR1 and CCR8 is particularly relevant for the development of small molecules against chemokine receptors. The observed differential role of ECL-2B for ligand potency and efficacy increases the influence of the extracellular regions on ligand binding and receptor activity – a field that will become increasingly relevant with the improved X-ray structures of these regions.

Acknowledgement

The studies were supported by The Danish Council for Independent Research | Medical Sciences, the NovoNordisk Foundation, the Lundbeck foundation, the European Community's Sixth Framework program (INNOCHEM: LSHB-CT-2005-518167), the AP-Moller Foundation and the Aase and Einar Danielsen Foundation.

Conflict of interest

There is no conflict of interest.

References

Alexander SPH, Mathie A, Peters JA (2011). Guide to Receptors and Channels (GRAC), 5th Edition. Br J Pharmacol 164 (Suppl. 1): S1–S324.

Allen SJ, Crown SE, Handel TM (2007). Chemokine: receptor structure, interactions, and antagonism. Annu Rev Immunol 25: 787–820.

Arias DA, Navenot JM, Zhang WB, Broach J, Peiper SC (2003). Constitutive activation of CCR5 and CCR2 induced by conformational changes in the conserved TXP motif in transmembrane helix 2. J Biol Chem 278: 36513–36521.

Baba M, Nishimura O, Kanzaki N, Okamoto M, Sawada H, Iizawa Y *et al.* (1999). A small molecule, nonpeptide CCR5 antagonist with highly potent and selective anti-HIV-1 activity. Proc Natl Acad Sci U S A 96: 5698–5703.

Baldwin JM (1993). The probable arrangement of the helices in G protein-coupled receptors. EMBO J 12: 1693–1703.

Ballesteros JA, Weinstein H (1995). Integrated methods for the construction of three-dimensional models and computational probing of structure-function relations in G protein-coupled receptors. Receptor Molecular Biology 25: 366–428.

Barth P, Wallner B, Baker D (2009). Prediction of membrane protein structures with complex topologies using limited constraints. Proc Natl Acad Sci U S A 106: 1409–1414.

Benned-Jensen T, Rosenkilde MM (2008). Structural motifs of importance for the constitutive activity of the orphan 7TM receptor EBI2: analysis of receptor activation in the absence of an agonist. Mol Pharmacol 74: 1008–1021.

Benned-Jensen T, Rosenkilde MM (2009). The role of transmembrane segment II in 7TM receptor activation. Curr Mol Pharmacol 2: 140–148.

Berkhout TA, Blaney FE, Bridges AM, Cooper DG, Forbes IT, Gribble AD *et al.* (2003). CCR2: characterization of the antagonist binding site from a combined receptor modeling/mutagenesis approach. J Med Chem 46: 4070–4086.

Black JW, Leff P (1983). Operational models of pharmacological agonism. Proc R Soc Lond 220: 141–162.

Bottegoni G, Kufareva I, Totrov M, Abagyan R (2009). Four-dimensional docking: a fast and accurate account of discrete receptor flexibility in ligand docking. J Med Chem 52: 397–406.

Bouvier M, Hnatowitch M, Collins SK, Kobilka B, Deblasi A, Lefkowitz RJ *et al.* (1988). Expression of a human cDNA encoding the b2-adrenergic receptor in Chinese hamster fibroblasts (CHW): functionality and regulation of the expressed receptors. Mol Pharmacol 33: 133–139.

Canutescu AA, Dunbrack RL (2003). Cyclic coordinate descent: a robotics algorithm for protein loop closure. Protein Sci 12: 963–972.

Castonguay LA, Weng Y, Adolfsen W, Di Salvo J, Kilburn R, Caldwell CG *et al.* (2003). Binding of 2-aryl-4-(piperidin-1-yl) butanamines and 1.3,4-trisubstituted pyrrolidines to human CCR5: a molecular modeling-guided mutagenesis study of the binding pocket. Biochemistry 42: 1544–1550.

Cherezov V, Rosenbaum DM, Hanson MA, Rasmussen SG, Thian FS, Kobilka TS *et al.* (2007). High-resolution crystal structure of an engineered human beta2-adrenergic G protein-coupled receptor. Science 318: 1258–1265.

Coutsias EA, Seok C, Wester MJ, Dill KA (2005). Resultants and loop closure. Int J Quantum Chem 1: 176–189.

Elling CE, Schwartz TW (1996). Connectivity and orientation of the seven helical bundle in the tachykinin NK-1 receptor probed by zinc site engineering. EMBO J 15: 6213–6219.

Farrens DL, Altenbach C, Yang K, Hubbell WL, Khorana HG (1996). Requirement of rigid-body motion of transmembrane helices for light activation of rhodopsin. Science 274: 768–770.

Gao P, Zhou XY, Yashiro-Ohtani Y, Yang YF, Sugimoto N, Ono S *et al.* (2003). The unique target specificity of a nonpeptide chemokine receptor antagonist: selective blockade of two Th1 chemokine receptors CCR5 and CXCR3. J Leukoc Biol 73: 273–280.

Gombert M, eu-Nosjean MC, Winterberg F, Bunemann E, Kubitza RC, Da Cunha L *et al.* (2005). CCL1-CCR8 interactions: an axis mediating the recruitment of t cells and langerhans-type dendritic cells to sites of atopic skin inflammation. J Immunol 174: 5082–5091.

Govaerts C, Blanpain C, Deupi X, Ballet S, Ballesteros JA, Wodak SJ *et al.* (2001). The TXP motif in the second transmembrane helix of CCR5. A structural determinant of chemokine-induced activation. J Biol Chem 276: 13217–13225.

Hall SE, Mao A, Nicolaidou V, Finelli M, Wise EL, Nedjai B *et al.* (2009). Elucidation of binding sites of dual antagonists in the human chemokine receptors CCR2 and CCR5. Mol Pharmacol 75: 1325–1336.

Haskell CA, Horuk R, Liang M, Rosser M, Dunning L, Islam I *et al.* (2006). Identification and characterization of a potent, selective nonpeptide agonist of the CC chemokine receptor CCR8. Mol Pharmacol 69: 309–316.

Hesselgesser J, Howard PN, Liang M, Zheng W, May K, Bauman JG *et al.* (1998). Identification and characterization of small molecule functional antagonists of the CCR1 chemokine receptor. J Biol Chem 273: 15687–15692.

Heydorn A, Ward RJ, Jorgensen R, Rosenkilde MM, Frimurer TM, Milligan G *et al.* (2004). Identification of a novel site within G protein alpha subunits important for specificity of receptor-G protein interaction. Mol Pharmacol 66: 250–259.

Hubbell WL, Altenbach C, Hubbell CM, Khorana HG (2003). Rhodopsin structure, dynamics, and activation: a perspective from crystallography, site-directed spin labeling, sulfhydryl reactivity, and disulfide cross-linking. Adv Protein Chem 63: 243–290.

Jaakola VP, Griffith MT, Hanson MA, Cherezov V, Chien EY, Lane JR *et al.* (2008). The 2.6 angstrom crystal structure of a human A2A adenosine receptor bound to an antagonist. Science 322: 1211–1217.

Jenkins TJ, Guan B, Dai M, Li G, Lightburn TE, Huang S *et al.* (2007). Design, synthesis, and evaluation of naphthalene-sulfonamide antagonists of human CCR8. J Med Chem 50: 566–584.

Jensen PC, Rosenkilde MM (2009). Chapter 8. Activation mechanisms of chemokine receptors. Methods Enzymol 461: 171–190.

Jensen PC, Nygaard R, Thiele S, Elder A, Zhu G, Kolbeck R *et al.* (2007). Molecular interaction of a potent nonpeptide agonist with the chemokine receptor CCR8. Mol Pharmacol 72: 327–340.

Jensen PC, Thiele S, Ulven T, Schwartz TW, Rosenkilde MM (2008). Positive versus negative modulation of different endogenous chemokines for CC-chemokine receptor 1 by small molecule agonists through allosteric versus orthosteric binding. J Biol Chem 283: 23121–23128.

Johnson GL, Bourne HR, Gleason MK, Coffino P, Insel PA, Melmon KL (1979). Isolation and characterization of S49 lymphoma cells deficient in b-adrenergic receptors:relation of receptor number to activation of adenylate cyclase. Mol Pharmacol 15: 16–27.

Kledal TN, Rosenkilde MM, Coulin F, Simmons G, Johnsen AH, Alouani S *et al.* (1997). A broad-spectrum chemokine antagonist encoded by Kaposi's sarcoma-associated herpesvirus. Science 277: 1656–1659.

Liang M, Mallari C, Rosser M, Ng HP, May K, Monahan S *et al.* (2000). Identification and characterization of a potent, selective, and orally active antagonist of the CC chemokine receptor-1. J Biol Chem 275: 19000–19008.

Luttichau HR, Stine J, Boesen TP, Johnsen AH, Chantry D, Gerstoft J *et al.* (2000). A highly selective CC chemokine receptor (CCR)8 antagonist encoded by the poxvirus molluscum contagiosum. J Exp Med 191: 171–180.

Maeda K, Das D, Ogata-Aoki H, Nakata H, Miyakawa T, Tojo Y *et al.* (2006). Structural and molecular interactions of CCR5 inhibitors with CCR5. J Biol Chem 281: 12688–12698.

Mandell DJ, Coutsias EA, Kortemme T (2009). Sub-angstrom accuracy in protein loop reconstruction by robotics-inspired conformational sampling. Nat Methods 6: 551–552.

de Mendonca FL, da Fonseca PC, Phillips RM, Saldanha JW, Williams TJ, Pease JE (2005). Site-directed mutagenesis of CC chemokine receptor 1 reveals the mechanism of action of UCB 35625, a small molecule chemokine receptor antagonist. J Biol Chem 280: 4808–4816.

Mirzadegan T, Diehl F, Ebi B, Bhakta S, Polsky I, McCarley D *et al.* (2000). Identification of the binding site for a novel class of CCR2b chemokine receptor antagonists: binding to a common chemokine receptor motif within the helical bundle. J Biol Chem 275: 25562–25571.

Mirzadegan T, Benko G, Filipek S, Palczewski K (2003). Sequence analyses of G-protein-coupled receptors: similarities to rhodopsin. Biochemistry 42: 2759–2767.

Mizuguchi K, Deane CM, Blundell TL, Overington JP (1998). HOMSTRAD: a database of protein structure alignments for homologous families. Protein Sci 7: 2469–2471.

Murphy PM, Baggiolini M, Charo IF, Hebert CA, Horuk R, Matsushima K *et al.* (2000). International union of pharmacology. XXII Nomenclature for chemokine receptors. Pharmacol Rev 52: 145–176.

Nygaard R, Frimurer TM, Holst B, Rosenkilde MM, Schwartz TW (2009). Ligand binding and micro-switches in 7TM receptor structures. Trends Pharmacol Sci 30: 249–259.

Palczewski K, Kumasaka T, Hori T, Behnke CA, Motoshima H, Fox BA *et al.* (2000). Crystal structure of rhodopsin: a G protein-coupled receptor. Science 289: 739–745.

Patel L, Charlton SJ, Chambers JK, Macphee CH (2001). Expression and functional analysis of chemokine receptors in human peripheral blood leukocyte populations. Cytokine 14: 27–36.

Peeters MC, van Westen GJ, Li Q, Ijzerman AP (2011). Importance of the extracellular loops in G protein-coupled receptors for ligand recognition and receptor activation. Trends Pharmacol Sci 32: 35–42.

Phillips R, Lutz M, Premack B (2005). Differential signaling mechanisms regulate expression of CC chemokine receptor-2 during monocyte maturation. J Inflamm 2: 14.

Rasmussen SGF, Choi HJ, Fung JJ, Pardon E, Casarosa P, Chae PS *et al.* (2011). Structure of a nanobody-stabilized active state of the [bgr]2 adrenoceptor. Nature 469: 175–180.

Rosenbaum DM, Cherezov V, Hanson MA, Rasmussen SG, Thian FS, Kobilka TS *et al.* (2007). GPCR engineering yields high-resolution structural insights into beta2-adrenergic receptor function. Science 318: 1266–1273.

Rosenkilde MM, Schwartz TW (2006). GluVII:06 – a highly conserved and selective anchor point for non-peptide ligands in chemokine receptors. Curr Top Med Chem 6: 1319–1333.

Rosenkilde MM, Cahir M, Gether U, Hjorth SA, Schwartz TW (1994). Mutations along transmembrane segment II of the NK-1 receptor affect substance P competition with non-peptide antagonists but not substance P binding. J Biol Chem 269: 28160–28164.

Rosenkilde MM, Benned-Jensen T, Frimurer TM, Schwartz TW (2010). The minor binding pocket – a major player in 7TM receptor activation. Trends Pharmacol Sci 12: 567–574.

Sabroe I, Peck MJ, Van Keulen BJ, Jorritsma A, Simmons G, Clapham PR *et al.* (2000). A small molecule antagonist of chemokine receptors CCR1 and CCR3. Potent inhibition of eosinophil function and CCR3-mediated HIV-1 entry. J Biol Chem 275: 25985–25992.

Scheerer P, Park JH, Hildebrand PW, Kim YJ, Krausz N, Choe HW *et al.* (2008). Crystal structure of opsin in its G-protein-interacting conformation. Nature 455: 497–502.

Schwartz TW (1994). Locating ligand-binding sites in 7TM receptors by protein engineering. Curr Opin Biotechnol 5: 434–444.

Schwartz TW, Rosenkilde MM (1996). Is there a 'lock' for all 'keys' in 7TM receptors. Trends Pharmacol Sci 17: 213–216.

Schwarz MK, Wells TN (2002). New therapeutics that modulate chemokine networks. Nat Rev Drug Discov 1: 347–358.

Seibert C, Ying W, Gavrilov S, Tsamis F, Kuhmann SE, Palani A *et al.* (2006). Interaction of small molecule inhibitors of HIV-1 entry with CCR5. Virology 349: 41–54.

Shi J, Blundell TL, Mizuguchi K (2001). FUGUE: sequence-structure homology recognition using environment-specific substitution tables and structure-dependent gap penalties. J Mol Biol 310: 243–257.

Strader CD, Sigal IS, Register RB, Candelore MR, Rands E, Dixon RA (1987). Identification of residues required for ligand binding to the beta-adrenergic receptor. Proc Natl Acad Sci U S A 84: 4384–4388.

Totrov M, Abagyan R (2008). Flexible ligand docking to multiple receptor conformations: a practical alternative. Curr Opin Struct Biol 18: 178–184.

Tsamis F, Gavrilov S, Kajumo F, Seibert C, Kuhmann S, Ketas T *et al.* (2003). Analysis of the mechanism by which the small molecule CCR5 antagonists SCH-351125 and SCH-350581 inhibit human immunodeficiency virus type 1 entry. J Virol 77: 5201–5208.

Vaidehi N, Schlyer S, Trabanino RJ, Floriano WB, Abrol R, Sharma S *et al.* (2006). Predictions of CCR1 chemokine receptor structure and bx 471 antagonist binding followed by experimental validation. J Biol Chem 281: 27613–27620.

Wang C, Bradley P, Baker D (2007). Protein-protein docking with backbone flexibility. J Mol Biol 373: 503–519.

Warne T, Serrano-Vega MJ, Baker JG, Moukhametzianov R, Edwards PC, Henderson R *et al.* (2008). Structure of a [bgr]1-adrenergic G-protein-coupled receptor. Nature 454: 486–491.

Warne T, Moukhametzianov R, Baker JG, Nehme R, Edwards PC, Leslie AGW *et al.* (2011). The structural basis for agonist and partial agonist action on a [bgr]1-adrenergic receptor. Nature 469: 241–244.

Wells TN, Power CA, Shaw JP, Proudfoot AE (2006). Chemokine blockers–therapeutics in the making? Trends Pharmacol Sci 27: 41–47.

Williams MG, Shirai H, Nagendra JHG, Mueller J, Mizuguchi K, Miguel RH *et al.* (2001). Sequence-structure homology recognition by iterative alignment refinement and comparative modeling. Proteins (Suppl. 5): 92–97.

Wu B, Chien EY, Mol CD, Fenalti G, Liu W, Katritch V *et al.* (2010). Structures of the CXCR4 chemokine GPCR with small molecule and cyclic peptide antagonists. Science 330: 1066–1071.

Zingoni A, Soto H, Hedrick JA, Stoppacciaro A, Storlazzi JA, Sinigaglia F *et al*. (1998). Cutting edge: the chemokine receptor CCR8 is preferentially expressed in Th2 but not Th1 cells1.2. J Immunol 161: 547–551.

Supporting information

Additional Supporting Information may be found in the online version of this article:

Figure S1 Screening for agonist activity of LMD-559 among endogenous chemokine receptors. IP_3 accumulation experiments performed in transiently transfected COS-7 cells. Dose–response curves for LMD-559 and a positive control selected amongst the possible endogenous agonists for all human chemokine receptors (except for CCR1 and CCR8, which are depicted in Figure 1). In addition, CCR11 was excluded, although no activation was observed for the non-peptide compound, as no endogenous ligand exists for this receptor (n = 3).

Figure S2 Screening for antagonism by LMD-559 amongst endogenous chemokine receptors. IP_3-accumulation experiments performed in transiently transfected COS-7 cells. The test for antagonism was performed by stimulation of each receptor with 10 nM of the depicted endogenous ligand. Dose–response curves for LMD-559 and a positive control are shown for the same receptors as in Figure S1 (n = 3).

Figure S3 Comparison of the minor binding pocket. The depth and expansion of the ligand-binding pocket is compared in four available crystal structures: CXCR4, Rhodopsin, β_2-adrenoceptor (ADR) and adenosine A_{2A} receptor. The top panel shows the receptors from the extracellular side, whereas the lower panel illustrates the receptors from the side as viewed from TM-VI and -VII, with the corresponding ligands shown in green sticks (It1t, retinal, carazolol and ZM241385 respectively). The binding pockets are illustrated with transparent space filling, and the minor binding pocket is highlighted with stippled lines.

Figure S4 LMD-559 modelling using the β_2-adrenoceptor (ADR) as template. The molecular modelling of LMD-559 in CCR8 (A,B) and in CCR1 (C,D) is presented as seen from above (A,C) and in a side view corresponding to the view from TM. The mirrored orientation of LMD-559 is apparent also in the modelling based on β2-ADR as template. Noticeable, the same key residues are identified as using CXCR4 as template and again corresponding to the residues identified by the mutational analyses. Importantly, the different roles of ECL-2B in the two receptors are confirmed. Thus, where it, in CCR1, seems to contribute directly to the binding site of LMD-559, it has a more indirect conformational constraining role in CCR8. This is indeed also apparent from the modelling based on β_2-adrenoceptor (B,D).

Figure S5 Extracellular view of small molecule binding in different receptors. The top panel display small molecule ligand binding in three different chemokine receptors (all based on the crystal structure of CXCR4). From the left: LMD-559 binding in CCR8, the mirrored binding of LMD-559 in CCR1 and It-1t in CXCR4. The lower panel displays three crystal structures solved when interacting with the small molecule ligands: retinal in Rhodopsin, carazolol in the β_2-adrenoceptor (ADR) and ZM241385 in the adenosine A_{2A} receptor. The group of structural water molecules that fill up the minor binding pocket in the A_{2A} receptor (Jaakola *et al*., 2008) is depicted in red sticks.

Please note: Wiley-Blackwell are not responsible for the content or functionality of any supporting materials supplied by the authors. Any queries (other than missing material) should be directed to the corresponding author for the article.